Technical Report No.: NGRI-2023-SEISM-3008

Geological & Geotechnical studies to understand shallow subsurface strata at Joshimath, Chamoli, Uttarakhand

Final Technical Report

Submitted to

Uttarakhand State Disaster Management Authority

Uttarakhand, Dehra Dun

By

CSIR-National Geophysical Research Institute

Uppal Road, Hyderabad, 500007

Team CSIR- National Geophysical Research Institute

1. Dr. Prakash Kumar, Director (Supervision)
2. Dr. Anand K. Pandey, Scientist (Overall responsibility & Coordination)
3. Dr. K. Satish Kumar, Scientist (MASW investigation)
4. Dr. [illegible] (GPR investigation)
5. Dr. Ved Prakash Maurya, Scientist (ERT investigation)
6. Dr. [illegible], Scientist (Ground deformation investigation)
7. Dr. Lalit Kumar – Technical Officer (ERT investigation)
8. Dr. S. Dinesh Kumar – Technical Officer (GIS, [illegible] and GPS)
9. Mr. B. Siva Shankar, Research Scholar (MASW investigation)
10. Miss. K. Swapna Sri, PA-II (MASW investigation)
11. Dr. M. J. [illegible], Scientist ([illegible] monitoring)

Acknowledgements

Sincere thanks to Dr. Ranjeet Sinha (Secretary, USDMA), Dr. Santanu Sarkar (Coordinator, USDMA), Dr. Piyoosh Rautela (Executive Director, USDMA), Mr. Himanshu Khurana (District Collector, Chamoli) and Dr. Virendra M. Tiwari (Outstanding Scientist, CSIR) for constant help, participation in discussions during and after field work. They have helped in focusing attention to the most relevant issues.

We acknowledge the use of open source SRTM DEM for landscape characterization, Sentinel remote sensing data and open source Python code for ground deformation studies.

Background

The Joshimath township in Chamoli district of Uttarakhand has been experiencing land subsidence problem and associated excess water discharge from the slope for past [illegible] during December 2022 – January 2023. The subsidence affected the habitation and infrastructure and the source of this excess discharge is not known. Taking cognizance of the developing phenomenon, the Uttarakhand State Disaster Management Authority (USDMA) contacted CSIR-National Geophysical Research Institute (vide letter no.: [illegible]/USDMA/[illegible] dated 8 January, 2023) attached as Annexure-I to undertake studies to determine the source of this water together with subsurface drainage and structures including crevasses and cracks to help in mitigation strategy.

In response, Director CSIR-NGRI deputed a team of scientists and Technical officers (vide letter no. [illegible] dated [illegible]) along with equipment to carry out an multiparametric geological and geophysical investigations. The team has expertise in shallow sub-surface investigation employing Remote sensing based ground deformation using SAR interferometry, geological mapping, Electric field Vertical Resistivity Imaging ([illegible]), Ground Penetrating Radar (GPR) and Multichannel Analysis of Surface Waves (MASW).

On request from USDMA, a proposal entitled "Geological & Geotechnical studies to understand the Shallow Subsurface Strata at Joshimath, Chamoli, Uttarakhand" detailing the scope, work plan and deliverables has been communicated. The same was approved by USDMA vide letter no. [illegible]/USDMA/[illegible] (2023) on 18 January 2023 with emphasis on "main focus of the study should be mapping of
underground water flow and nature of subsurface geology".

Scope of work:

Mapping of shallow subsurface using [illegible], MASW, GPR techniques and geological characterisation of slope instability.

Objectives:

Following broader objectives were proposed:

1. Preparation of structural and geological maps through satellite imageries and detailed geological mapping
2. Generation of 2D/3D geophysical images related to subsurface.
3. Integration of MASW, GPR and [illegible] data sets for potential zones.
4. Comprehensive report.

Executive Summary

The CSIR-NGRI team carried out field investigations on above objectives and the findings are summarized in order. The details of each study are separately summarized in subsequent sections.

1. The N-dipping Joshimath slope is a dip-slope where the inclination (dip) of the rock basement and slope are in same direction.
2. The slope comprises of thick loose soil derived from modified older landslide debris and glacio-fluvial deposits which lies over the N-dipping basement Gneissic [illegible] rocks of the [illegible] Formation.
3. The Joshimath slope constitutes of disjointed patches of [illegible] gentle slopes that are bordered by steep slopes producing series of benches. The gentle slopes have regolith cover of variable thickness. These gentle slopes are mostly occupied for habitation and subsistence agriculture.
4. The Joshimath slope have experienced [illegible] differential subsidence with [illegible] (estimated Line of Site (LOS) subsidence) during December 2022-January 2023. The peak subsidence regions have experienced development of fissures with variable and large (up to ~1m) horizontal and vertical subsidence. The subsidence caused extensive damage to houses and properties including infrastructures.
5. The ground fissure pattern suggests a narrow subsidence zone corresponding to the zone identified in InSAR data.
6. The Electrical Resistivity Tomography (ERT) survey covering different part of the Joshimath slope reveals the concave [illegible] of regolith cover with variable thickness, which often exceeds ~50 m adjacent to the streams or rivulets on the slope. The high resistivity basement rocks also have narrow zones of fracture where the ground water is channelised, especially towards the toe region.
7. The multichannel analysis of Shear waves (MASW) profiles covering subsidence zone suggests the regolith cover has low and higher velocity [illegible] thickness of layers [illegible] with variable [illegible] thickness. The top 5-15m low velocity layer is [illegible] with Vs [illegible], followed by 10-20m thick [illegible] and with a [illegible] underlying [illegible] layer over the basement of Consolidated/Hard Rock formation with a velocity of > 700m/s.
8. The thick low velocity layer [illegible] of [illegible] derived from old landslide debris material is more prominent at Marwari, Narsingh Mandir, Joshimath and Rope Way area.

The distribution of this low velocity layer should be considered for safety measures, though the beds are not prone to liquefaction.

9. The ERT survey confirms the stratification with the 2nd higher density layer, which preserves the soil moisture, whereas the low velocity sediments are devoid of saturation. The steep, un-filled fissures are extensively developed and extends to a depth ~10m. The fissures become gentler and shallower in the saturated slope at the toe of Joshimath, where the ephemeral subsurface discharge was observed [illegible] during subsidence.

10. The subsidence caused disappearance of minor surface discharges (rivulets) in the fissure affected zones. The surface runoff direction (NNE) doesn't match the subsurface flow driven discharge at the toe zone in WNW direction.

11. The depth slices of shear wave velocity (Vs) distribution, derived by interpolation and contouring of observed MASW profiles, suggest the ~22 m thick sediment column at the upper slope region, such as Marwari bag, show NE flow accumulation like the surface runoff direction. Whereas, the some >10m depth slices subsurface flow accumulation in WW direction as observed in the field where of disappearance of rivulets and ephemeral sub-soil discharge near the lower JP road.

12. The fissures act as [illegible] connections to the subsurface flow and help in channelization of [illegible], which is observed in the ephemeral sub-soil discharge during subsidence.

13. On the basis of overlay analysis of different thematic layers, we defined two risk zones for the present Joshimath subsidence. We considered the boundary defined by InSAR subsidence and the field observations as limits of the risk zones. The fissure distribution are comparing well with the peak subsidence zone where deep-seated subsurface flow was channelizing the surface runoff and decreasing of the soil column at a depth ~20-30 m in the regolith thickness is defined as High risk zone (marked in orange color overlaid with blue arrow). The other zone (marked in yellow) experienced moderate subsidence without [illegible] the development of fissures or ground subsidence involving <12 m of regolith cover with similar subsurface flow and surface runoff is defined as Moderate risk zone.

The detailed observations and inferences are presented in subsequent sections.

INTRODUCTION

The Uttarakhand has been frequented by disastrous landslides, avalanches, cloudbursts, floods & earthquakes and the ground subsidence. Some notable events of mass wasting during past century are: (i) the 1893 Gohna landslide and the 1894 & 1970 Gohna GLOF along the Birahi Ganga river in the Alaknanda (ii) the 1979 [illegible] landslide blockade of the Bhagirathi (iii) the 1998 Okhimath landslide in the Madhyamaheshwar Ganga (iv) the 2013 Kedarnath cloudburst and flashflood (v) Rishi Ganga rockfall driven glacio-fluvial deluge along Rishi Ganga prior to the January 2023 subsidence in the Joshimath.

Table 1.1: Some notable catastrophic events of Uttarakhand

Year	Name of the catastrophe	Condition
[illegible]	Bhagirathi blocked	
[illegible]	Alaknanda blocked for three days	GLOF - [illegible]
[illegible]	Alaknanda slide	[illegible]
[illegible]	Flooding in Bhagirathi	Bridges devastated
[illegible]	Nainital landslide	
[illegible]	Birahi Ganga blocked near Gohna	Formation of Gohna Tal [illegible]
[illegible]	Partial breach of Gohna lake	Bridges swept, level of Ganga rises [illegible] Haridwar, [illegible]
[illegible]	Dhauli Ganga blocked	LGOF
[illegible]	Rishi Ganga blocked	GLOF
[illegible]	Rainfall near Joshimath	20 km of the road washed
[illegible]	[illegible] damming of [illegible] Ganga	[illegible]
[illegible]	Bhagirathi blocked by landslide	GLOF
[illegible]	[illegible] (Alaknanda flood)	GLOF/Massive devastation downstream up to Haridwar
[illegible]	[illegible] Ganga blocked	
[illegible]	[illegible], Bhagirathi blocked	GLOF
[illegible]	Bhagirathi blocked between [illegible] and [illegible]	GLOF
1998	Okhimath slide	More than 100 dead, massive loss of property due to GLOF
1998	Malpa slide	More than 200 dead, 1st batch of Mansarovar yatra pilgrims
[illegible]	Varunavat landslide in Uttarkashi	
[illegible]	[illegible]	
2013	Kedarnath flash flood	More than 5000 killed and massive damage in downstream, GLOF
2021	[illegible] avalanche & Dhauli Ganga flash floods	More than 200 were killed & [illegible]
2023	Joshimath Subsidence	[illegible] houses and agriculture fields [illegible], development of ground fissures, disappearance of surface runoff along small streams and [illegible] discharge [illegible]

The region surrounding Joshimath experienced catastrophic landslide triggered glacier flash flood deluge on 7th February 2021 and extreme precipitation of ~200mm during 17-19 October 2021 on the Joshimath slope. Though the scattered subsidence and development of cracks in the residential structures are being reported for over a year (since November 2021) in Sunil ward in different parts, but a large part of the Joshimath township started subsiding in the first week of January 2023 and subsidence has not abated since (Fig. 1). The subsidence is accompanied by disappearance of surface discharge in streams and gushing of silt-rich sediment discharge at the JP Marwari area towards the northwestern toe region of the Joshimath slope.

Fig. 1. Google image of the north facing slope of Joshimath township. The ground subsidence and development of large ground fissures are mostly observed in the built-up area, such as Sunil, Manohar Bag, Singhdhar, Marwari JP and near Narsingh temple areas.

The report aimed understanding cause of subsidence phenomenon by characterising thickness of loose soil/regolith, the saturation pattern, stiffness characteristics of soil and geometry of the fissures in parts of Joshimath, which has witnessed similar subsidence decades ago. The Mishra committee submitted report in year 1976 considered the prior landslide material in the region as a major cause of slope instability (No. [illegible] dated [illegible] April 1976). Since the Joshimath is an important route connecting Badrinath, Hemkund Sahib, Auli and Valley of Flowers and forward posts along Sino-Indian border in the east of the country, its stability is important.

Joshimath, in the Chamoli district of Uttarakhand, lies at an elevation between [illegible] m above msl (Fig. 2) on the left flank of the Alaknanda river. The widespread development of ground fissures produced cracks in >[illegible] houses until [illegible] Jan. 2023 has created confusion and social unrest among inhabitants.

Fig. 2: The topography of Joshimath region.

GEOLOGY OF THE REGION

Joshimath township is situated in the Higher Himalaya where the crystalline rocks of Vaikrita Group lie tectonically over the Lesser Himalayan crystallines of Munsiari Group rocks along the Vaikrita Thrust (Valdiya, 1980; Fig. 3). The hillslope of Joshimath is made up of medium to high grade metamorphic rocks of the Central Crystallines comprising of weakly and banded gneiss and schist, which are exposed at the base of the Joshimath town, adjacent to the riverbed. The northerly dip slope of the Joshimath, where the northerly dipping crystalline rocks of the

[illegible]

Fig. 3 Geology of the [illegible]

GROUND SUBSIDENCE (SATELLITE BASED SAR INTERFEROMETRY)

[illegible]

Data and method

[illegible]

includes backgeocoding, assist in coregistering the two SLC products of same sub swath using orbit files and DEM. The enhanced spectral diversity process was done to estimate a constant azimuth shift between the images, which minimises the phase discontinuities across the bursts. After compensating the azimuth offset, interferogram was generated. Deburst processing is done to merge number of bursts in the azimuth direction to form seamless image. The topographic phase component in the raw interferometric phase were removed using the geometry of the InSAR and DEM to compensate the topographic effect. The resultant phase includes phase signatures related to deformation.

The interferograms were filtered using Goldstein phase nonlinear adaptive filtering (Goldstein and Werner, 1998) followed by multi-looking (4×1), which improves the wrapped phase accuracy. Wrapped interferometric phase is unwrapped using snaphu tool (SNAPHU, 2002). The unwrapped differential phase value (radians) is converted to the displacement value (in meters) along the line of sight (LOS) of the sensor. The geometric correction was done using the range Doppler terrain correction operator geometrically corrects SAR data and provides the ground displacement map (Fig. 4). Data fusion techniques were used to derive the vertical velocity by combining LOS measurements from two independent InSAR viewing geometries (i.e., Ascending and Descending). The vertical velocity is derived by fusing ascending and descending LOS measurements using Fuhrmann & Garthwaite, 2019 on a pixel by pixel basis.

Fig. 4. SAR Interferometry based ground deformation in the Line of Site (LOS) of the satellite using time-lapse repeat observation.

Results

The land subsidence map using DInSAR data for the period of 15th December 2022 to 15th January 2023 (Fig 4) suggests the subsidence phenomenon started during start of December 2022 and continued during January 2023. The negative values indicate the LOS subsidence, i.e. typically moving away from the camera during the period of satellite observations. The subsidence values are ~4-6cm between the 15-27 December 2022 reduced to 2-4cm by 15th January 2023. There was no subsidence observed at the end of January 2023. The subsidence was observed in the middle and western side of the Joshimath area, although isolated subsidence observed throughout the Joshimath area. The subsidence proceeded towards the eastern slopes with the peak subsidence in 2019-2022 trending eastward area.

The land-cover analysis of satellite data reveals that percentage of built-area footprint increased from 1.23 sq.km to 2.3 sq.km between 2010-2020 doubled in last decade (2012 to 2022), which is 100% increase per decade. It is obvious to expect that the rapid growth of built-up area would put tremendous pressure cause subsidence to demand and supply chain of water potential, large scale building of sanitation pits and would destabilized the nearby area buildings scenario.

GROUND FISSURE MAPPING

We carried out a detailed mapping of the fissures in the Joshimath township (Fig. 3). The fissures are mapped in the barren agriculture fields, along the road and the floor of buildings etc. The fissures are distributed from the upper slopes at ~2200m in Sunil region to the Marwari/JP region at the toe of the Joshimath slope at ~1400m with the map pattern (Fig. 3) show a close correlation along the identified subsidence zones (Fig. 4). The vertical displacement varies from centimeter to decimeter scale and fissure openings up to 30 cm wide are observed.

Fig. 3: The ground fissure distribution in the Joshimath township.

Based on the field observations, the mapped area has been divided into 5 (five) blocks namely, a) Sunil, b) Manohar Bagh, c) Singhdhar, d) Marwari, and e) Narsingh Mandir.

a) **Sunil ward**: located on the northern uphill slopes of Joshimath along the Auli road, has been experiencing slope creeping and fissures development for over an year with the confirmed representation to district administration was submitted in November 2021. The impressions of creeping is manifested in the man-made structures in the form of buckling of retaining walls, backtilting of the concrete structure opposite to the slope. The second fissures have appeared in January 2023 with the ground movement including ruptures extending into houses as cracks due to unequal settlement of houses etc. (Fig. 6). The fissures [illegible] created a E-W trending [illegible] fissures perpendicular to the slope were observed, [illegible] eastward. Sunil Dhar is a part of Sunil ward, located opposite to Sunil. Moving further eastward, the orientation of the surface ruptures takes a N-S direction perpendicular to the direction of the slope. Indications of active movement of the surface beneath these structures.

Fig. 6: Field observations of cracks and bulging in Sunil ward.

b) **Manohar Bagh**: located on the National Highway-7 constitutes the main Joshimath township, which is severely affected with development of extensive ground fissures affecting buildings. The fissures show 0-50 cm vertical displacement and upto 30 cm horizontal displacement (Fig. 7). The general trend of fissures are E-W direction parallel to the slope with few more N-S trending fissures (perpendicular to the slope) observed towards the eastern margin around Singhdhar.

Fig. 7: Ground fissures at Manohar bagh road in the Joshimath township with extensive damages to the houses.

c) Singhdhar witnessed extensive development of ground fissures ranging from 50 cm to 1 m vertical and horizontal displacements (Fig. 8). The observed fissures are oriented in E-W direction parallel to the slope.

d) Marwari & JP colony, located in the northern side towards the Alaknanda river, region is affected with the ground fissures developed parallel to the slope (Fig. 8). Towards the base of the slope, a large area with the forest/ thick vegetation cover shows creeping, as marked by tilting of the trees. The zone experienced major displacement of ~1m, which had impacted the structures in the vicinity. The toe region experienced gushing of groundwater of unknown origin with the peak discharge as high as >500 lpm (Fig. 9), which gradually decreased in a week. The discharge picked up again on 20-21 January 2023 after the fresh snow fall and rain and subsided in next two days to almost nil flow with a few tens litre per minute.

e) Narsingh Mandir section shows incipient development of minor ground fissures with centimetre displacement and minor cracks in the buildings and retaining walls. The minor fissures, in comparison to the rest of the region, indicates unstable slope that should not be neglected. Further, the above below lower slopes, adjacent to the Joshimath town, show creep and gully erosion.

Fig. 4 Large fractures and ground deformations are observed adjacent to the [illegible] region, where [illegible] the merging of [illegible] zone. The [illegible] on the [illegible] [illegible] [illegible] [illegible] [illegible].

Fig. 5. The fractures and [illegible] made ground [illegible] [illegible] which [illegible] also [illegible] [illegible] [illegible] zones.

Fissure Pattern

We analysed the displacement (height and width) along the fissures in order to understand the area wise pattern of the surface subsidence of Joshimath slope (Fig. 11). The maximum horizontal displacement along the fissures are observed in parts of Sunil, Manoharbagh and Singhdhar with displacement as high as 45 cm (Fig. 11a), whereas the vertical displacement as high as 100-150 cm, are observed in Singhdhar and Marwari-JP region (Fig. 11b).

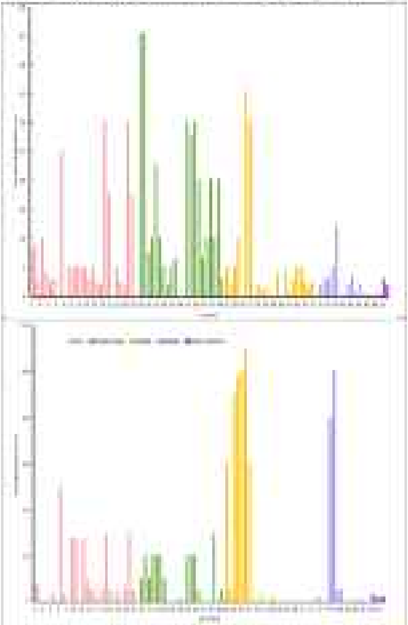

Fig. 10 Horizontal and vertical displacement of the ground along the fissures.

Fissure localization vs geomorphic landform

It was observed that the larger displacement along the fissures are confined to the region having thick sediment cover in comparison to the hardrock area. To understand the fissure localization, we analysed the geomorphology evolution of the [illegible] slope. We used open source SRTM Digital Elevation Model (DEM) of 30m spatial resolution. We also used 12.5m spatial resolution ALOS Palsar DEM, but results were similar. We generated slope and slope aspect maps of the [illegible] region (Fig. 11) and overlaid them with the drainage, fissure distributions and the buildup area.

Three [illegible] flowing streams and their [illegible] dissect the [illegible] slope. The slope is dissected with a series of gentle slope regions [illegible] in general trending in E-W direction and separated by high slope ridges. The gentle sloping segments in the [illegible] (B) and [illegible] (C) areas are highly infested with the fissures. The fissures distribution is arcuate and the transverse fissures adjacent to the NNW trending [illegible] defines the prominent slope break and margin of the fissure dislocation (Fig. 11) during present subsidence. The lower gentle slope around [illegible] (B), further NE [illegible], has experienced development of fissures with large displacement (Fig. [illegible]).

The [illegible] appears to be an important geomorphic discontinuity as observed in the slope aspect map. It is important to note that the middle stream is originating from [illegible] whereas the other channels towards east and west are originating from the [illegible] slope (Fig 11).

Summary

- The ground deformation with development of fissures and subsidence is observed.
- The fissures are mostly confined to the gently sloping built-up areas.
- The fissure segments have vertical displacement correlating with the peak subsidence zone as observed in the InSAR data analysis.
- The fissures show characteristic displacement; the vertical displacement is prominent in [illegible], whereas the horizontal displacement is prominent at the upper and mid reaches of the subsidence zone.
- The major subsidence zone is bounded by the NNW trending [illegible], which also controls the surface runoff as observed in the drainage.

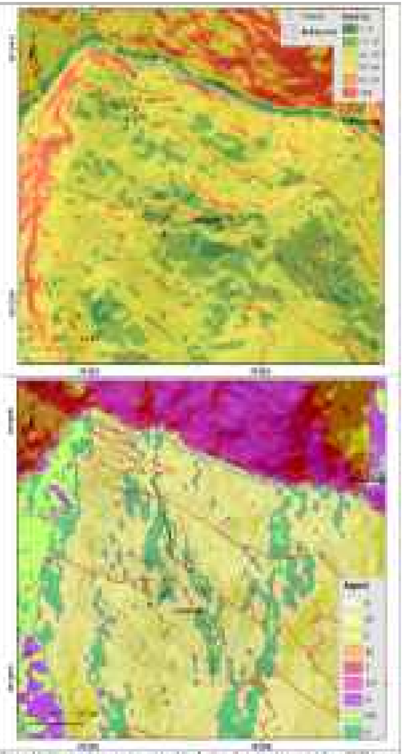

Figure 11: Slope and slope aspect map of the [illegible] region (generated from SRTM DEM of 30 m spatial resolution) in.

MULTI-PROXY GEOPHYSICAL CHARACTERIZATION OF SHALLOW SUBSURFACE SUBSTRATE

The surface runoff of a few minor channels has disappeared during Joshimath subsidence and the sudden gush of sediment-laden discharge near JP colony in Marwari was a surprise as the location is not aligned to the northward natural slope and flow of the surface water (Fig 11). This points towards the possibility of the channelization of N flowing surface water towards SW direction through subsurface flow. Further, the presence of a [illegible] of perched water table in the cause and trigger of subsidence in Joshimath was commonly discussed among the experts and policy makers with frequent media coverage. To evaluate the hypothesis, it is imperative to map the *thickness & subsurface configuration of the loose overburden on the Joshimath slope, which is deforming and channelizing the subsurface flow?*

In view of high relative relief and strongly sloping rugged terrain of Joshimath, we planned and used Electrical resistivity survey (ERT), Multichannel Analysis of Surface Waves (MASW) and Ground Penetrating Radar (GPR) techniques for shallow subsurface exploration with specific objectives. The ERT survey along ~1km long profiles with ~100m depth coverage would help in finding depth and geometry of overburden regolith with the basement across the subsidence affected areas. The MASW (~50m) profiles would help in constraining the stiffness characteristics of soil and stratification in ~50m regolith section in the subsidence areas. The GPR is employed to map subsurface geometry and extent of fissures and detail saturation pattern of the soil column up to a depth of ~20-40m. The understanding from these methods will be integrated with the geological observations to constrain subsidence behaviour and subsurface flow pattern in the Joshimath slopes.

A. Electrical survey over Joshimath region

The electrical surveys are conducted for the Joshimath area with an altitude variation of 1400-2000 m (Figure 12). The resistivity profiles were spread ~1 km in length with an electrode spacing of ~25 m. These profiles are almost parallel to the elevation contours following the almost E-W trending roads. The altitude difference between these roads are very high with no connectivity in the N-S steeply sloping direction (~40-70 deg), restricting our surveys along the roads. In total, 10 voltage receiver units have been placed for each profile. The multiple current injections were done in the profile direction to cover the area with substantial resolution. The decoupled voltage and current units helped us in data acquisition for such extremely challenging mountainous terrain. Usually, contact resistances were adjusted up to orders of some kilo-ohms (~5kΩ). Such high contact resistances are observed and consistent with the exposed hard rocks in the region. Also, we tried to inject a substantial amount of currently (~1000 m) [illegible] using two [illegible] potential transmitters (in total ~ [illegible] and 3000 V) for greater depth of investigation (reaching up to a maximum of ~ 150-200 m depth) and good data quality. At each node, two potential dipoles were measured along the profile direction with a dipole length of ~ 25 m. Finally, the recorded voltage (in order of some millivolts to hundreds of millivolts) and current waveforms are processed to provide the apparent resistivity data.

Figure 2.[illegible]: [illegible] survey field layout map for the [illegible] area. [illegible] position along the four ERT profiles [illegible]

The resistivity models are prepared along the four ERT profiles (Figs. [illegible]) after removing the acquired data points with anomalous error than of ~ [illegible] % and an absolute voltage error of ~ 0.1 mV. The mesh with millions of tetrahedral cells were used in the model space with ~ 200 Ωm background resistivity as starting model. The background resistivity is the average of the acquired resistivity data. In horizontal direction, [illegible] cells are included in the model, and in vertical direction, the model cell size was kept ~ [illegible] m. The topography was also included precisely in the models based on the updated SRTM [illegible] spatial resolution DEM of the [illegible] region. The obtained resistivity models have marked some pronounced resistive and conductive anomalous patterns.

Four major domains were recognized from the resistivity distribution, i.e.,

(i) highly conductive saturated fine sand silt ([illegible] Ωm);
(ii) the saturated unconsolidated conductive sediments ([illegible] Ωm);

iii) moderately resistive basement granitic rocks (100-500 Ωm); and
iv) resistive exposed rocks and boulders occurrences (> 500 Ωm)

The results suggest the unconsolidated soft rocks (conductive sediments) mostly confined to a depth < 150 m. Some shallow conductive anomalies possibly show the existence of the saturated fracture/fault. At places, shallow resistive anomalies exist and represent the big boulders distribution in the region. There are exposed hard rocks visible at the surface also consistent in the obtained resistivity models. The possible distribution of the interface between the basement and unconsolidated soft sediments are clearly marked in the models. Some shallow resistive and conductive anomalies are correlated with the observed lateral displacement in the field.

The resistivity signatures of all the four profiles in Bandl Ghera, Mandore Bagh, Ukhrul Manda and IIT & Marwari village are discussed below in further details.

1. Bandl Ghera area

In Bandl Ghera area, a resistive rock mass thick pile of unconsolidated sediments was identified (Fig. 11). The general geometry of low resistive zones extending the ... small channel affecting the exposed mass with weathering and deposition of regolith. The western side of the section (near the ERT range) is mostly hard rocks with some narrow weak zones. At places weak zones are consistent with mapped location of the faults.

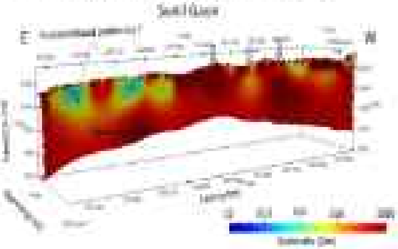

Figure 12: Resistivity model section along the ERT profile in Bandl Ghera area with the subsurface zones (gray shaded vertical arrows) in the lower zone as in figure 12.

II. Upper Mandhar Bagh area along the Juili road

There is indication of a clear-cut boundary between unconsolidated sediments and basement rocks in the Mandhar Bagh profile (Fig. 14). These sediments are as thick as about 70-80 meters depths in the central portion. It becomes relatively thin in the western side as basement goes up steep and occasionally resistive boulders are also seen. The locations of the cracks mostly persistent in the eastern side of this profile. It is also located more closely to the highly damaged area by subsidence process.

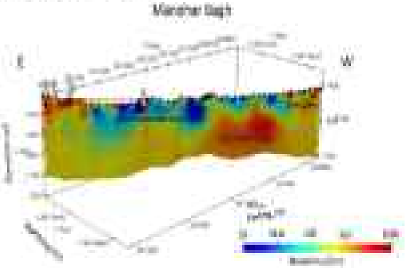

Figure 14: Resistivity cross-section along the ERI profile in Mandhar Bagh area with the [illegible] (grey shaded vertical section) [illegible] figure 13. Red dotted rectangle shows the locations of the dense cluster of [illegible] < 100 m.

III. Narsingh Mandir

The profile starts near the Singdhar road in the east and extends towards the Narsingh Mandir area in the west (Fig. 15). At the east, unconsolidated sediments becomes thinner as compared to central portion, where it reaches up to 70-80 meters. At places, resistive hard rocks are exposed to the surface. Also, some deeper weak zones are identified in the western and close to the Singdhar road.

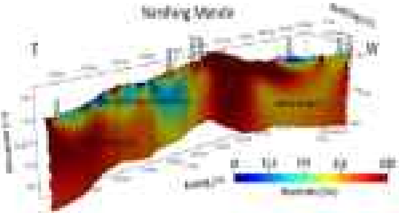

Figure 12: [illegible]

[illegible]

[illegible]

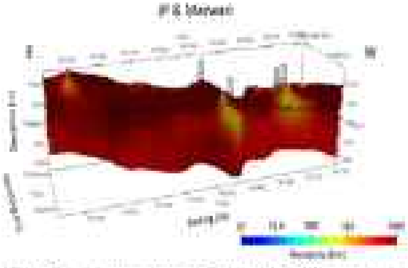

Figure 13: [illegible]

Summary

- The regolith cover is not uniform across Jharkhand.
- The overburden occur in the form of [illegible] with the maximum thickness [illegible] observed around [illegible] streams.
- The regolith cover of [illegible] m around [illegible] and [illegible] areas and laterally extends for [illegible]m.
- The fissures are mostly observed in the areas with thick regolith cover; however, the margin areas are also affected by subsidence fissures.
- At [illegible] area, the basement is exposed near the surface with certain narrow areas of [illegible]. This [illegible] the emergence of subsurface groundwater flow as ephemeral large discharge during subsidence.

B. Multichannel Analysis of Surface Waves (MASW) Studies

It is important to determine the subsurface soil characteristics in Joshimath region to understand the site condition and site response of soil stratification during ground subsidence and future hazards. The MASW is a well-established geophysical method to determine shear wave velocity distribution of the shallow subsurface geological layers and it provides input parameters to the civil and structural engineers for safety aspect of the civil structures. We acquired MASW data along twelve profiles in and around subsidence area identified from satellite images and field identification of damaged (Fig. 17). The planned length of each profile is 100 m, which varies depending on the availability of free space to lay the equipment. The shear wave velocity (Vs) was mapped up to a depth of 20 m to 40 m from the surface. The following subsurface soil parameters are estimated from MASW study:

1. 2D shear wave velocity structure of the subsurface layers
2. Average velocities (Vs) at a depth interval of 5m, 10m, 15m, 20m, 25m and 30m (Vs 5 to Vs 30)
3. Classification of the Subsurface in the terms of National Earthquake Hazard Reduction Program (NEHRP)
4. Stiffness of the Soils
5. Predominant Frequency and Amplification of soils.
6. Liquefaction Potential/ Factor of safety

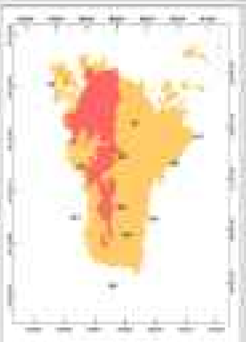

[illegible]

Methodology:

In most surface seismic surveys, the two-thirds of total seismic energy generated, using a compressional wave source, is imparted into Rayleigh waves (Richart, et al., 1970), which is the principal component of ground roll. Although ground roll is considered as noise on body wave surveys (i.e., reflection or refraction profiling), its dispersive properties can be utilized to infer near-surface elastic properties (Stokoe, et al., 1988; Nazarian, et al., 1994; Park, et al., 1999a). Assuming vertical velocity variation, each frequency component of a surface wave has a different propagation velocity (called phase velocity, Cf) at each unique frequency component (f), which results in different wavelength. Further, a series of Rayleigh waves of different frequencies can have the same velocity. These different phase velocities of Rayleigh waves for a given frequency are known as modes. The lowest velocity for any given frequency is called the fundamental mode velocity. The next higher velocity above the fundamental mode phase velocity is called second mode velocity and so on. The fundamental phase velocities when calculated with high accuracy will generally provide reliable shear-wave velocities (Park, et al., 1999 and Xia, et al., 2000). Construction of a shear (S)-wave velocity (Vs) profile through the analysis of plane-wave, fundamental-mode Rayleigh waves is one of the most common way to use the dispersive properties of surface waves (Bullen, 1963). This analysis provides key parameters commonly used to evaluate near-surface stiffness, which is a critical property for geotechnical studies (Stokoe, et al., 1994).

The shear wave velocity (Vs) of a medium is a function of the elastic properties and is directly related to the stiffness of the materials (Table B1). The Vs are used to compute harmonic mean shear wave velocity, stiffness, predominant frequency, amplification and liquefaction potential for the study area, which is important parameter to assess the quality of the rock for civil engineering constructions and estimation of liquefaction hazard potential in seismically active region. Harmonic shear wave velocity over the top 30 m is referred to as V_s^{30}. Both the National Earthquake Hazard Reduction Programme (NEHRP) provisions and the Uniform Building Code (UBC) classification (of 1997) use V_s^{30} to classify sites according to type of soil for earthquake engineering design (Table B2; Dobry, et al., 2000; Kanli, et al., 2006).

Table B1: Seismic Velocities for different rock types

Rock Type	Formation	P-wave Velocity (Vp), m/s	S-Wave Velocity (Vs), m/s
Very Hard Rock	Fresh granite, Basalt, Quartzite and limestones	>5000	>1500
Rock	Amphibolites, Shale, Slate, Lime stone, Marble and Phyllites etc.	2000 to 5000	750-1500
Dense Soils and Soft rock	Semi Weathered granite, Basalt, Dolomite, Shale and Clay stone/Sand Stone etc.	1000 to 2000	360-750
Stiff Soils	Completely Weathered rock, Chalk, Black Soil, Gravel, Laterite etc.	500 to 1000	180-360
Soft Soils	Loose, Sediment, Sand, Clay, Sediments	<500	<180

Table 06: Soil profile type classification for seismic amplification (BSSC, 2003)

Soil Type NEHRP	Formation	Average Shear Wave Velocity in 30 m (V_{s30}), m/s
A	Hard Rock	>1500
B	Rock	760 < V_s ≤ 1500
C	Very Dense Soils and Soft rock	360 < V_s ≤ 760
D	Stiff Soils	180 ≤ V_s ≤ 360
E	Soft Soils	≤ 180
F	Soils requiring site specific evaluations	

Liquefaction is defined as the transformation of a granular material from solid to a liquefied state because of increased pore water pressure that reduces effective stress. The occurrence of liquefaction depends upon the amplitude and duration of the ground shaking and the depth of the water table. In general, older soils have a lower liquefaction potential. Soils at depths of more than 15m generally do not liquefy due to the high effective confining pressure.

Field Data acquisition and Processing:

The MASW field data was acquired along the [illegible] profiles, i.e. Profiles [illegible] to [illegible] (Fig. 17, Table 07). The seismic pulses were generated through 8kg sledge hammer as a source, 4.5Hz vertical geophones used as receiver and multi-purpose seismic recorder with 24 channels Geode (seismograph: Geometrics make) to record the signals (Fig. 18). During acquisition sampling interval and record length were taken as [illegible] msec and [illegible] sec and notch filter applied to avoid the recording of electrical signal from any unknown underground source. We not set a filter for acquisition [illegible] to allow all types of frequencies recorded from the different formation.

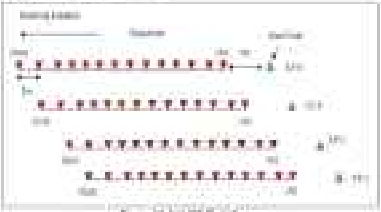

Figure 18: MASW Field Set up

Table 8A: MASW Acquisition Parameters					
Profile No	Spread Length/Surface Coverage, m	Station Interval, m	Sample Interval, ms	Record Length, sec	Profile direction
[illegible]	100	2	0.25	1	West-East
[illegible]	100	2	0.25	1	West-East
[illegible]	100	2	0.25	1	West-East
[illegible]	100	2	0.25	1	East-West
[illegible]	100	2	0.25	1	East-West
[illegible]	100	2	0.25	1	[illegible]
[illegible]	100	2	0.25	1	West-East
[illegible]	100	2	0.25	1	West-East
[illegible]	100	2	0.25	1	West-East
[illegible]	100	2	0.25	1	West-East
[illegible]	100	2	0.25	1	West-East
[illegible]	100	2	0.25	1	West-East

The raw seismic data, preprocessed, dispersion curve and inversion images are presented (Fig. 3 in Annexure-III). The same procedure repeated for acquiring all data sets. The acquired seismic data are processed using "surfseis software" (KGS make). The seismic data processing involves conversion of SEG-2 data to KGS format, assignment of geometry (in this study offset [illegible] and group interval [illegible] has been chosen), filtering of geometry assigned data (e.g. [illegible] mute to nullify the first arrival and multiples respectively), generation of dispersion curve, extraction of dispersion curve, inversion of dispersion image to get the 1D shear wave velocity image of each record and generation of 2D shear wave velocity image by combining of the 1D shear wave velocity images. Accurate generation of dispersion curve is one of the critical factors in the estimation of shear wave velocity profile.

Results:

The data from individual profiles (12 nos.) are processed following above protocol and the profile images with salient observations along them are presented in the Annexure-III. The general property along the profiles are summarized in Table 8B and Fig. 19.

Average Shear Wave Velocity (Vs) and associated Geotechnical parameters:

The Vs is varying from 200 to 700 m/s throughout the region from 0m to 30m. The observed average shear wave velocity (from 0 m to 30m depths) at each site ([illegible] to [illegible]) are interpolated by using minimum curvature technique. The average Shear wave velocity (Vs) images and corresponding NEHRP soil classification from 0m to 30m depths in the subsidence region are plotted (Fig. 20). According to classification of sites based on ([illegible] to Vs-30) is given by Federal Emergency Management Agency (FEMA) (1997) and Uniform Building

Code (IBC-ICBC, 1997), the Subansiri region is consists of "Stiff soils (Class D) and Very dense soil and soft rock (Class C)". Stiff Soil are observed up to the depth of 5m followed by a dense soil up to the depth of 40 m. A very hard rock is observed below the 70 m. The average shear wave velocity distribution from 5m to 70 m also presented.

The stiffness of the soil is varying from [illegible] KN/m to [illegible] KN/m. The proportionality is observed in stiffness of the rocks with shear wave velocity. Predominant frequencies and Amplifications of the soils varies from 1.0 Hz to 2 Hz and 0.7 to 1.5 throughout the [illegible] area. The estimated Liquefaction factor [illegible] with reference to maximum earthquake of [illegible] Mw ([illegible] earthquake) with PGA of [illegible] (Table [illegible]).

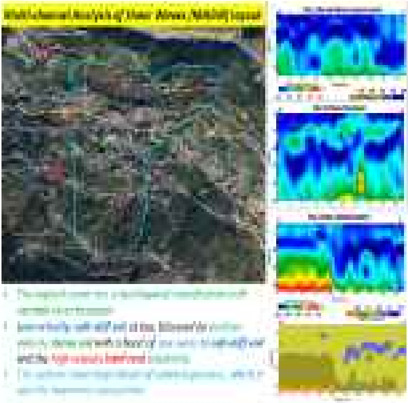

Fig. 10: Average picture of MASW analysis and output summary. The details of each profile are given in Annexure III.

[illegible]

[illegible]	[illegible]	[illegible]	[illegible]	[illegible]	[illegible]	[illegible]	[illegible]	[illegible]
[illegible]	[illegible]	[illegible]	[illegible]	[illegible]	[illegible]	[illegible]	[illegible]	[illegible]
[illegible]	[illegible]	[illegible]	[illegible]	[illegible]	[illegible]	[illegible]	[illegible]	[illegible]
[illegible]	[illegible]	[illegible]	[illegible]	[illegible]	[illegible]	[illegible]	[illegible]	[illegible]
[illegible]	[illegible]	[illegible]	[illegible]	[illegible]	[illegible]	[illegible]	[illegible]	[illegible]
[illegible]	[illegible]	[illegible]	[illegible]	[illegible]	[illegible]	[illegible]	[illegible]	[illegible]
[illegible]	[illegible]	[illegible]	[illegible]	[illegible]	[illegible]	[illegible]	[illegible]	[illegible]
[illegible]	[illegible]	[illegible]	[illegible]	[illegible]	[illegible]	[illegible]	[illegible]	[illegible]
[illegible]	[illegible]	[illegible]	[illegible]	[illegible]	[illegible]	[illegible]	[illegible]	[illegible]
[illegible]	[illegible]	[illegible]	[illegible]	[illegible]	[illegible]	[illegible]	[illegible]	[illegible]

[illegible]	[illegible]	[illegible]	[illegible]	[illegible]	[illegible]	[illegible]	[illegible]	[illegible]	[illegible]	[illegible]
[illegible]	[illegible]	[illegible]	[illegible]	[illegible]	[illegible]	[illegible]	[illegible]	[illegible]	[illegible]	[illegible]
[illegible]	[illegible]	[illegible]	[illegible]	[illegible]	[illegible]	[illegible]	[illegible]	[illegible]	[illegible]	[illegible]
[illegible]	[illegible]	[illegible]	[illegible]	[illegible]	[illegible]	[illegible]	[illegible]	[illegible]	[illegible]	[illegible]
[illegible]	[illegible]	[illegible]	[illegible]	[illegible]	[illegible]	[illegible]	[illegible]	[illegible]	[illegible]	[illegible]
[illegible]	[illegible]	[illegible]	[illegible]	[illegible]	[illegible]	[illegible]	[illegible]	[illegible]	[illegible]	[illegible]
[illegible]	[illegible]	[illegible]	[illegible]	[illegible]	[illegible]	[illegible]	[illegible]	[illegible]	[illegible]	[illegible]
[illegible]	[illegible]	[illegible]	[illegible]	[illegible]	[illegible]	[illegible]	[illegible]	[illegible]	[illegible]	[illegible]
[illegible]	[illegible]	[illegible]	[illegible]	[illegible]	[illegible]	[illegible]	[illegible]	[illegible]	[illegible]	[illegible]
[illegible]	[illegible]	[illegible]	[illegible]	[illegible]	[illegible]	[illegible]	[illegible]	[illegible]	[illegible]	[illegible]
[illegible]	[illegible]	[illegible]	[illegible]	[illegible]	[illegible]	[illegible]	[illegible]	[illegible]	[illegible]	[illegible]
[illegible]	[illegible]	[illegible]	[illegible]	[illegible]	[illegible]	[illegible]	[illegible]	[illegible]	[illegible]	[illegible]

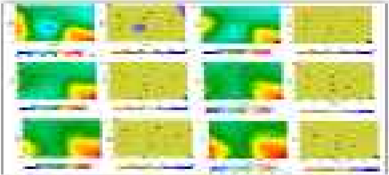

Conclusions of MASW studies:

The shear wave velocity of 12 profiles in and around [illegible] results:

- The irregular multi-layered stratification is observed in the [illegible] [illegible] occur throughout the [illegible] area. The layering are not uniform and show local variation.
- The shear wave velocity (Vs) of the soil layers varies from <180 to >750 m/s up to a depth of 30 m.
- The top 3-10 m low velocity layer is soft-stiff soil with Vs<[illegible] m/s, followed by [illegible] thick stiff/dense soil with a thin underlying stiff-[illegible] layer, over the basement of [illegible] formation with a velocity of >700 m/s.
- The discrete low velocity layer <180 m/s (soft soil) is variously composed of [illegible] material. This low velocity is more prominent at [illegible], [illegible] and [illegible] areas in [illegible].
- The [illegible] have large blocks (often <10m in dimension) of [illegible] rocks, which have Vs similar to the basement horizon.
- The distribution of this low velocity layer at depth should be consider for safety measures.

C. Ground Penetration Radar (GPR) *(Mapping fissure geometry and saturation)*

The Ground Penetrating Radar (GPR) survey has been employed to understand saturation characteristics of the top soil and fissure geometry in the subsidence zone. The GPR survey was conducted along adjacent to the ERT and MASW profiles (Fig. 21) for any correlation.

Figure 21. Layout Map of GPR Profiles (GP-1 to GP-[illegible]) overlaid on the Google Image.

The GPR field data was acquired along the [illegible] profiles (Fig 21), i.e., Profiles from GP-1 to GP-[illegible] in and around the subsidence region covering the Marwari, Jail road, Sunil area, Manohar Bag, Ropeway, Paramgh Mandir, Singhdhar Road and JP road. The location and lengths of each profile is listed in Table-[illegible].

The acquired GPR data has been processed using Reflexw software following the protocol presented in the Annexure-IV. The results of the 2-D observations are marked in the form of 2-D profiles (Fig. 22), which are presented in Annexure-IV. Some salient observations are summarised under:

- Top soil up to a depth of [illegible] is poorly saturated.

- A partially saturated regolith with soil moisture is invariably observed between 5-15 m depth. This soil moisture layer corresponds well to the higher velocity dense soil of MASW.
- The lower sections around the streams are showing good soil moisture.
- Highly saturated zones are observed Marwari, Singdhar, Mandhar Bagh, Kundi, and JP area mostly along the surface-subsurface water flow (riverine) regions.
- However, the dry soil, less filled soil column (visible as bright white-yellow colour) are common towards the margins of flow zones.
- Margins of subsidence zone and upper reaches are showing moisture due to depth of fissures are notified in the regolith layer.

Table C1: Details of GPR profile

P.No	Village name	Latitude	Longitude	Latitude	Longitude	Profile direction
JG-1	Marwari	[illegible]	[illegible]	[illegible]	[illegible]	West-East
JG-2	Marwari	[illegible]	[illegible]	[illegible]	[illegible]	West-East
JG-3	Marwari	[illegible]	[illegible]	[illegible]	[illegible]	West-East
JG-4	Singdhar Road	[illegible]	[illegible]	[illegible]	[illegible]	West-East
JG-5	Singdhar Road	[illegible]	[illegible]	[illegible]	[illegible]	West-East
JG-6	Singdhar Road	[illegible]	[illegible]	[illegible]	[illegible]	West-East
JG-7	Singdhar Road	[illegible]	[illegible]	[illegible]	[illegible]	West-East
JG-8	Narsing Mandir	[illegible]	[illegible]	[illegible]	[illegible]	West-East
JG-9	Narsing Mandir	[illegible]	[illegible]	[illegible]	[illegible]	West-East
JG-11	Manoharbagh	[illegible]	[illegible]	[illegible]	[illegible]	West-East
JG-12	Manoharbagh	[illegible]	[illegible]	[illegible]	[illegible]	West-East
JG-13	Manoharbagh	[illegible]	[illegible]	[illegible]	[illegible]	West-East
JG-14	Manoharbagh	[illegible]	[illegible]	[illegible]	[illegible]	West-East
JG-15	Manoharbagh	[illegible]	[illegible]	[illegible]	[illegible]	West-East
JG-16	Manoharbagh	[illegible]	[illegible]	[illegible]	[illegible]	West-East
JG-17	Sunil Road	[illegible]	[illegible]	[illegible]	[illegible]	West-East
JG-18	Sunil Road	[illegible]	[illegible]	[illegible]	[illegible]	West-East
JG-19	Sunil Road	[illegible]	[illegible]	[illegible]	[illegible]	West-East
JG-20	Sunil Road	[illegible]	[illegible]	[illegible]	[illegible]	West-East
JG-21	Sunil Road	[illegible]	[illegible]	[illegible]	[illegible]	West-East
JG-22	Sunil Road	[illegible]	[illegible]	[illegible]	[illegible]	West-East
JG-23	Sunil Road	[illegible]	[illegible]	[illegible]	[illegible]	West-East
JG-24	J.P. Road	[illegible]	[illegible]	[illegible]	[illegible]	West-East
JG-25	J.P. Road	[illegible]	[illegible]	[illegible]	[illegible]	West-East
JG-26	Ropeway	[illegible]	[illegible]	[illegible]	[illegible]	West-East
JG-27	Ropeway range	[illegible]	[illegible]	[illegible]	[illegible]	North-South

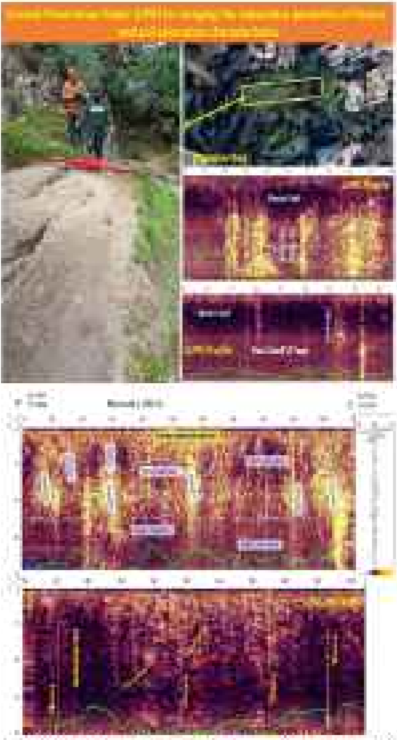

Fig. 22: GPR profiles along different fissure induced region of Joshimath. [illegible]

[illegible]

- Minor to major fissures are better manifested in partially saturated soils. The distribution of fissures and cracks are independent to individual regions.
- Shorter, but filled, vertical fissures are frequently observed in the higher reaches.
- The fissures are as deep as ~15 m, though depth and geometry of fissures varies in the saturated soil zones (marked in black and purple colour) and fissures thickness and tapered at 15-20 m depth towards lower reaches.

INTEGRATION AND DISCUSSION

It is imperative to integrate the multiparametric observation from the remote sensing, geological and geophysical techniques to understand the ground subsidence phenomenon in the Joshimath. It is important to summarize the critical observations and inferences from the studies and look for the inferred answer.

The salient observation from the present study can be summarized as:

- The Joshimath is north facing dip slope, where the basement is constituted of north dipping gneissic rocks of [illegible] Formation (Fig. 5).
- The slope is segmented with a series of [illegible] gentle slopes are separated by steep slopes forming [illegible] benches.
- The SAR interferometry results for the December 2022 and January 2023 is able to map a well-defined subsidence zone with higher subsidence towards the western flank (Fig. 9), where the ground fissures and building damage are observed (Fig. 7-8, Annexure II).
- The deep fissures are frequent with large horizontal displacement in the gentle slope areas in Sunil, Manohar Bag and Singh Dhar areas (Fig. 10). The larger vertical displacement is common in Singh Dhar and Marwari-JP areas (Fig. 10).
- The north facing dip slope of Joshimath is segmented with variable regolith cover thickness as observed in ERT study (Fig. 15-20). The gentle sloping areas (Fig. 11) around Sunil have regolith thickness of >60m, forming [illegible] pockets [illegible] independent sliding zones connected to slope aspects and are separated by the shallow basement rocks (Fig. 15-18).
- The regolith has 5-8 m [illegible] soil [illegible] of variable thickness are observed over the hard, un-weathered basement rocks (Fig. 11, 20, Annexure III).
- A large set of fissures has developed in the overburden regolith. The fissures extend to ~10 m depth with variable geometry. The fissures are often air filled in the upper middle slopes and are having a shallower [illegible] geometry towards the toe region around Marwari and JP (Fig. 22, Annexure IV). The stiff dense middle soil layer in MASW (Fig 20) is able to hold soil moisture (Fig. 22) but are devoid of saturation in upper middle slopes.

However, the following enhanced landform and runoff change needs explanation considering shallow sub-surface observations of the present study.

- The gushing of slowish water from the lower toe end of the slope at kilometre-59 road has occurred simultaneously with the Sukhanidi subsidence during initial days of subsidence.
- Several small rivulets with minor surface runoff disappeared during the Sukhanidi subsidence.
- The short and precipitation on 20-21 January 2022 produced the enhanced water discharge at the [illegible] near [illegible], which disappeared in next couple of days.
- This suggests the disappearance of disappeared surface runoff as subsurface flow. However, there is no [illegible] representing surface runoff follow the same geometry.

It raises a question, whether subsurface water (groundwater) flow is different from surface runoff, and how?

To deal with the above question, it is important to understand the nature of the Sukhanidi slope, which is constituted of degraded [illegible] gentle slope bordered by steep slopes forming series of benches (Fig. 11). The subsidence affected slope (A, B, C, D areas) are degraded small catchments have distinct flow pattern are bordered by the [illegible] (Fig. 22), which seems to control channelization of the surface runoff along the rivulets and gravity subsurface flow as well. The slope and aspects map of the region clearly suggests that the [illegible] acts as the [illegible] to the [illegible] diverted surface runoff.

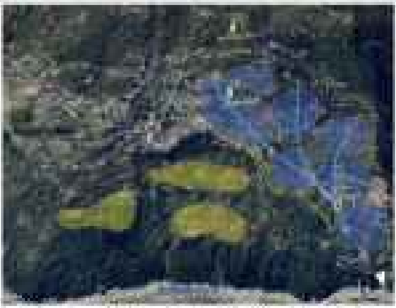

Fig. 22: Google image of the Sukhanidi slope overlaid with the small catchments. The LIDAR DEM (being generated by other agency) would give better resolution.

We modeled the flow accumulation pattern of the Joshimath slope using SRTM DEM of 30m spatial resolution (Fig. 29), which clearly suggest the dominant surface flow is in NNE direction, which is obstructed by the SW-ward flow pattern of Singhdhar. The InSAR based subsidence (Fig. 4) and fissure pattern (Fig. 5) also suggest the northwestwardly subsidence bordered by the Singh Dhar. The sediment transport flow at Marwari was observed during 20-22 January 2023 spell of snow and precipitation on Joshimath slope. The disappearance of NE-N flowing rivulets in the upper slope produced sediment transport discharge at Marwari during subsidence suggests a northwestwardly subsurface flow (Fig. 23, 24).

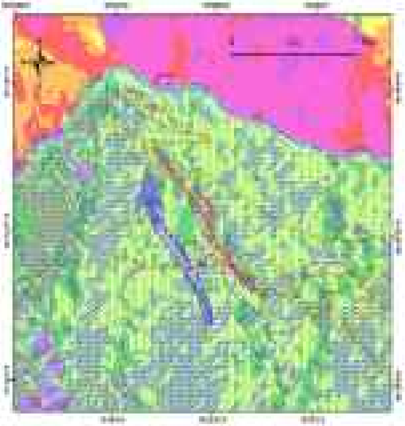

Fig. 29: Flow accumulation pattern (derived from SRTM 30m spatial resolution) of the Joshimath slope representing the direction of surface runoff. Please note the direction of subsidence and the subsurface runoff as observed at Marwari towards NW direction. The Singh Dhar with SW flow direction acts as barrier to the NE-N directed surface flow of the slope.

To understand the subsurface flow behaviour, we converted the depth slices of Vs derived from MASW analysis with an assumption that the Vs contours at 5, 10, 15, 20, 25 and 30m depths would help in constructing a broad picture of subsurface geometry of the road/rocks and soils similar property (Fig. 23). The convergence zone of TL contours will broadly point towards flow accumulation at that depth. It is interesting to note that the TL contour convergence pointing a flow path, which changes from NE direction up to 15m depth and to NW direction at deeper levels.

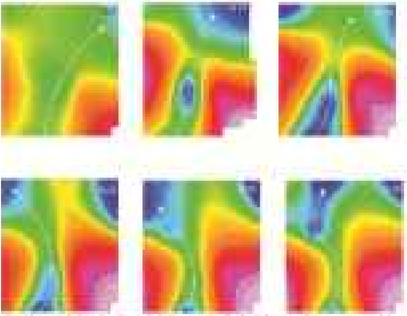

Fig. 23. Horizontal MASW profiles sliced at different depth distribution of Shear wave Velocity (Vs). Please note the contour convergence portions a varying flow path identify the subsurface accumulation would be in NE direction up to 15m depth and it changes to NW direction at deeper levels.

It appears, continuing in light of ~40 m deeper Tension in the upper slope region of Joshimath (Fig. 25, Appendix-IV) would channelise disappearing surface runoff to the NW directed subsurface flow, as observed during subsidence.

Further, the baseline discharge at JP-Marwari slope has progressively decreased from ~550lpm to ~17 lpm (negligible) unless a drought and presence of air-filled fissures at ~20-25 m depth points towards serious loosening of the regolith (overburden) due to enhanced base flow along the basement-overburden interface. The seasonal revival of enhanced discharge after a short spell of rain-snow on 20-21 January 2023 also suggests that the subsidence and associated subsurface discharge is not over yet.

It would encourage a qualified guess to consider the Joshimath subsidence as a recurring phenomenon, which is continuing. Possibly the behavior of the slope subsidence and discharge during the forthcoming monsoon season [illegible] would [illegible] the [illegible] of present subsidence phenomenon.

Risk Zone

We combined all the above observations to demarcate the affected areas with various degree of risk with variable soil column thickness (Fig. [illegible]) with the understanding that the risk and vulnerability will be higher in thicker vulnerable soil column. We define two risk zones with boundary defined by InSAR subsidence and the field observations. The fissures distributions are [illegible] well with the peak subsidence zone and therefore we define it as High-risk zone, affected by a deeper subsurface [illegible] flow involving [illegible] of regolith thickness. The other zone experienced uniform subsidence without [illegible] development of fissures or ground subsidence is defined as Moderate risk zone where the subsurface flow is similar to the surface runoff and it affects [illegible] m of regolith cover.

References

Building Seismic Safety Council (BSSC), (2000). NEHRP Recommended Provisions for Seismic Regulations for New Buildings and Other Structures, Parts 1 and 2, FEMA-368, Federal Emergency Management Agency, Washington, D.C.

Bullen, K.E., (1963). An introduction to the theory of seismology; Cambridge Univ. Press.

Dobry, R., Borcherdt, R.D., Crouse, C.B., Idriss, I.M., Joyner, W.B., Martin, G.R., Power, M.S., Rinne and Seed, R.B., (2000). New site coefficients and site classification system used in recent building seismic code provisions, Earthquake Spectra, 16, No. 1, pp 41-67, February.

Federal Emergency Management Agency (FEMA), 1997. Multi Hazard Identification and Assessment. FEMA, Washington, D.C.

Kanli, A.I., Tildy, P., Prónay, Z., Pinar and Hermann, L., (2006). VS 30 mapping and soil classification for site effect evaluation in Dinar region, SW Turkey, Geophysical J. Int., Vol. 165, pp 223-235.

Nazarian, S., Stokoe II, K. H., and Hudson, W. R., (1983). Use of spectral analysis of surface waves method for determination of moduli and thickness of pavement systems, Transportation Research Record No. 930, 38-45.

Park, C.B., Xia, J., and Miller, R.D., (1998a). Ground roll as a tool to image near-surface anomaly: 68th Ann. Internat. Mtg., Soc. Expl. Geophys., Expanded Abstracts, p. 874-877.

Park, Choon B., Miller, Richard D., Xia, Jianghai., (1999). Multichannel analysis of surface waves. Geophysics 64 (3), 800-808.

Richart, F.E., Hall, J.R., and Woods, R.D., (1970). Vibrations of soils and foundations: Prentice-Hall, Inc.

Stokoe, K. H. II, Wright, S. G., Bay, J. A., and Roesset, J. M. (1994). Characterization of geotechnical sites by SASW method, in Geophysical characterization of sites, ISSMFE Technical Committee #10, edited by R. D. Woods, Oxford Publishers, New Delhi.

Valdiya, K.S. 1980. Geology of Kumaun Lesser Himalaya. WIHG publication.

Xia, J., Miller, R. D. and Park, C. B., (2000). Advantages of Calculating Shear Wave Velocity from Surface Waves with Higher Modes, SEG, 70th Annual Meeting, Calgary, Alberta, Canada, 1295-1298.

Annexure

Geological & Geotechnical studies to understand shallow subsurface strata at Joshimath, Chamoli, Uttarakhand

Draft Report Summary

Submitted to

Uttarakhand State Disaster Management Authority

Uttarakhand, Dehra Dun

By

CSIR-National Geophysical Research Institute

Uppal Road, Hyderabad 500007

Technical Report No.: NGRI-2023-[illegible]

Appendix 2

No. [illegible]

From,

Additional Chief Executive Officer (Administration)

Uttarakhand State Disaster Management Authority

Uttarakhand Secretariat, Dehradun

To,

The Director

CSIR – NGRI, Hyderabad

Dehradun

Dated [illegible] January 2023

Dear Sir,

As requested by the District Administration, the area in and around [illegible] in Chamoli district of Uttarakhand is facing land subsidence related problems and the issue has been aggravated by water flowing out of the [illegible] around [illegible]. So far the source of this water has not been ascertained.

We understand that National Geophysical Research Institute has both manpower and equipment to [illegible] in order to determine the source of this water, together with [illegible] and [illegible] [illegible].

You are accordingly requested to constitute a team of Scientists to undertake this study. The state government would be extending all logistic support to the visiting CSIR – NGRI team. Information of the [illegible] of the [illegible] to this office would be appreciated.

Yours sincerely,

[illegible]

([illegible])

ACEO (Administration)

Copy to the following for information and further necessary action:

1. Secretary, Hon'ble Chief Minister for the information of Hon'ble Chief Minister Ji.
2. Secretary, Disaster Management, Government of Uttarakhand.
3. [illegible] Secretary, National Disaster Management Authority, New Delhi.
4. District Magistrate, Chamoli.

([illegible])

ACEO (Administration)

CSIR - NATIONAL GEOPHYSICAL RESEARCH INSTITUTE

Council of Scientific & Industrial Research

[illegible]

[illegible]

Dear Sir,

Sub: [illegible]

[illegible]

1. Dr. [illegible]
2. Dr. [illegible]
3. Dr. [illegible]
4. [illegible]
5. [illegible]
6. [illegible]
7. [illegible]
8. [illegible]
9. [illegible]
10. [illegible]

[illegible]

Thanking you,

[illegible]

No. [illegible]

From,

Secretary
Disaster Management and Rehabilitation,
Govt. of Uttarakhand.

To,

Director,
CSIR – NGRI,
Hyderabad

Dehradun: Dated: 13 January, 2023

Subject: Approval of proposed [illegible] in Joshimath Town.

Dear Sir,

Please take reference to this office letter No. [illegible] dated [illegible] January, 2023, [illegible] "Geological and Geotechnical studies to understand the [illegible]" [illegible] following terms:

1. The [illegible]
2. The [illegible]
3. [illegible]
4. The Institute is requested to submit the [illegible] immediately.

As the matter is highly important, therefore it is requested to commence the work immediately.

Sincerely,

(Dr. Ranjit Kumar Sinha)
Secretary

Copy to following for information and necessary action:-

1. Secretary to Hon'ble Chief Minister, Uttarakhand.
2. Member Secretary, National Disaster Management Authority (NDMA), Govt. of India.
3. Joint Secretary, Ministry of Home, Govt. of India.
4. Divisional Commissioner, Garhwal.
5. Additional Chief Executive Officer [illegible], Uttarakhand State Disaster Management Authority.
6. District Magistrate, Chamoli.

(Dr. Ranjit Kumar Sinha)
Secretary

[illegible]

[illegible]	[illegible]	[illegible]	[illegible]	[illegible]				[illegible]	
				[illegible]	[illegible]		[illegible]	[illegible]	[illegible]
A	1	[illegible]	[illegible]	[illegible]	[illegible]	[illegible]	[illegible]	[illegible]	[illegible]
	[illegible]	[illegible]	[illegible]	[illegible]	[illegible]	[illegible]	[illegible]	[illegible]	[illegible]
	[illegible]	[illegible]	[illegible]	[illegible]	[illegible]	[illegible]	[illegible]	[illegible]	[illegible]
	[illegible]	[illegible]	[illegible]	[illegible]	[illegible]	[illegible]	[illegible]	[illegible]	[illegible]
	[illegible]	[illegible]	[illegible]	[illegible]	[illegible]	[illegible]	[illegible]	[illegible]	[illegible]
	[illegible]	[illegible]	[illegible]	[illegible]	[illegible]	[illegible]	[illegible]	[illegible]	[illegible]
	[illegible]	[illegible]	[illegible]	[illegible]	[illegible]	[illegible]	[illegible]	[illegible]	
	[illegible]	[illegible]	[illegible]	[illegible]	[illegible]	[illegible]	[illegible]	[illegible]	[illegible]
	[illegible]	[illegible]	[illegible]	[illegible]	[illegible]	[illegible]	[illegible]	[illegible]	[illegible]
	[illegible]	[illegible]	[illegible]	[illegible]	[illegible]	[illegible]	[illegible]	[illegible]	[illegible]
	[illegible]	[illegible]	[illegible]	[illegible]	[illegible]	[illegible]	[illegible]	[illegible]	[illegible]
	[illegible]	[illegible]	[illegible]	[illegible]	[illegible]	[illegible]	[illegible]	[illegible]	[illegible]
	[illegible]	[illegible]	[illegible]	[illegible]	[illegible]	[illegible]	[illegible]	[illegible]	[illegible]
	[illegible]	[illegible]	[illegible]	[illegible]	[illegible]	[illegible]	[illegible]	[illegible]	[illegible]
	[illegible]	[illegible]	[illegible]	[illegible]	[illegible]	[illegible]	[illegible]	[illegible]	[illegible]
	[illegible]	[illegible]	[illegible]	[illegible]	[illegible]	[illegible]	[illegible]	[illegible]	[illegible]
	[illegible]	[illegible]	[illegible]	[illegible]	[illegible]	[illegible]	[illegible]	[illegible]	[illegible]
	[illegible]	[illegible]	[illegible]	[illegible]	[illegible]	[illegible]	[illegible]	[illegible]	[illegible]
	[illegible]	[illegible]	[illegible]	[illegible]	[illegible]	[illegible]	[illegible]	[illegible]	[illegible]
	[illegible]	[illegible]	[illegible]	[illegible]	[illegible]	[illegible]	[illegible]	[illegible]	[illegible]
	[illegible]	[illegible]	[illegible]	[illegible]	[illegible]	[illegible]	[illegible]	[illegible]	[illegible]
	[illegible]	[illegible]	[illegible]	[illegible]	[illegible]	[illegible]	[illegible]	[illegible]	[illegible]
B	[illegible]	[illegible]	[illegible]	[illegible]	[illegible]	[illegible]	[illegible]	[illegible]	[illegible]
	[illegible]	[illegible]	[illegible]	[illegible]	[illegible]	[illegible]	[illegible]	[illegible]	[illegible]
	[illegible]	[illegible]	[illegible]	[illegible]	[illegible]	[illegible]	[illegible]	[illegible]	[illegible]
	[illegible]	[illegible]	[illegible]	[illegible]	[illegible]	[illegible]	[illegible]	[illegible]	[illegible]
	[illegible]	[illegible]	[illegible]	[illegible]	[illegible]	[illegible]	[illegible]	[illegible]	[illegible]
	[illegible]	[illegible]	[illegible]	[illegible]	[illegible]	[illegible]	[illegible]	[illegible]	[illegible]
	[illegible]	[illegible]	[illegible]	[illegible]	[illegible]	[illegible]	[illegible]	[illegible]	[illegible]
	[illegible]	[illegible]	[illegible]	[illegible]	[illegible]	[illegible]	[illegible]	[illegible]	[illegible]

[illegible]																				[illegible]													
[illegible]	[illegible]	[illegible]	[illegible]	[illegible]	[illegible]	[illegible]	[illegible]	[illegible]	[illegible]	[illegible]	[illegible]	[illegible]	[illegible]	[illegible]	[illegible]	[illegible]	[illegible]	[illegible]	[illegible]	[illegible]	[illegible]	[illegible]	[illegible]	[illegible]	[illegible]	[illegible]	[illegible]	[illegible]	[illegible]	[illegible]	[illegible]	[illegible]	[illegible]
[illegible]	[illegible]	[illegible]	[illegible]	[illegible]	[illegible]	[illegible]	[illegible]	[illegible]	[illegible]	[illegible]	[illegible]	[illegible]	[illegible]	[illegible]	[illegible]	[illegible]	[illegible]	[illegible]	[illegible]	[illegible]	[illegible]	[illegible]	[illegible]	[illegible]	[illegible]	[illegible]	[illegible]	[illegible]	[illegible]	[illegible]	[illegible]	[illegible]	[illegible]
[illegible]	[illegible]	[illegible]	[illegible]	[illegible]	[illegible]	[illegible]	[illegible]	[illegible]	[illegible]	[illegible]	[illegible]	[illegible]	[illegible]	[illegible]	[illegible]	[illegible]	[illegible]	[illegible]	[illegible]	[illegible]	[illegible]	[illegible]	[illegible]	[illegible]	[illegible]	[illegible]	[illegible]	[illegible]	[illegible]	[illegible]	[illegible]	[illegible]	[illegible]
[illegible]	[illegible]	[illegible]	[illegible]	[illegible]	[illegible]	[illegible]	[illegible]	[illegible]	[illegible]	[illegible]	[illegible]	[illegible]	[illegible]	[illegible]	[illegible]	[illegible]	[illegible]	[illegible]	[illegible]	[illegible]	[illegible]	[illegible]	[illegible]	[illegible]	[illegible]	[illegible]	[illegible]	[illegible]	[illegible]	[illegible]	[illegible]	[illegible]	[illegible]
[illegible]	[illegible]	[illegible]	[illegible]	[illegible]	[illegible]	[illegible]	[illegible]	[illegible]	[illegible]	[illegible]	[illegible]	[illegible]	[illegible]	[illegible]	[illegible]	[illegible]	[illegible]	[illegible]	[illegible]	[illegible]	[illegible]	[illegible]	[illegible]	[illegible]	[illegible]	[illegible]	[illegible]	[illegible]	[illegible]	[illegible]	[illegible]	[illegible]	[illegible]
[illegible]	[illegible]	[illegible]	[illegible]	[illegible]	[illegible]	[illegible]	[illegible]	[illegible]	[illegible]	[illegible]	[illegible]	[illegible]	[illegible]	[illegible]	[illegible]	[illegible]	[illegible]	[illegible]	[illegible]	[illegible]	[illegible]	[illegible]	[illegible]	[illegible]	[illegible]	[illegible]	[illegible]	[illegible]	[illegible]	[illegible]	[illegible]	[illegible]	[illegible]
[illegible]	[illegible]	[illegible]	[illegible]	[illegible]	[illegible]	[illegible]	[illegible]	[illegible]	[illegible]	[illegible]	[illegible]	[illegible]	[illegible]	[illegible]	[illegible]	[illegible]	[illegible]	[illegible]	[illegible]	[illegible]	[illegible]	[illegible]	[illegible]	[illegible]	[illegible]	[illegible]	[illegible]	[illegible]	[illegible]	[illegible]	[illegible]	[illegible]	[illegible]
[illegible]	[illegible]	[illegible]	[illegible]	[illegible]	[illegible]	[illegible]	[illegible]	[illegible]	[illegible]	[illegible]	[illegible]	[illegible]	[illegible]	[illegible]	[illegible]	[illegible]	[illegible]	[illegible]	[illegible]	[illegible]	[illegible]	[illegible]	[illegible]	[illegible]	[illegible]	[illegible]	[illegible]	[illegible]	[illegible]	[illegible]	[illegible]	[illegible]	[illegible]
[illegible]	[illegible]	[illegible]	[illegible]	[illegible]	[illegible]	[illegible]	[illegible]	[illegible]	[illegible]	[illegible]	[illegible]	[illegible]	[illegible]	[illegible]	[illegible]	[illegible]	[illegible]	[illegible]	[illegible]	[illegible]	[illegible]	[illegible]	[illegible]	[illegible]	[illegible]	[illegible]	[illegible]	[illegible]	[illegible]	[illegible]	[illegible]	[illegible]	[illegible]

	[illegible]	[illegible]	[illegible]	[illegible]	[illegible]	[illegible]	[illegible]	[illegible]	[illegible]
	[illegible]	[illegible]	[illegible]	[illegible]	[illegible]	[illegible]	[illegible]	[illegible]	[illegible]
	[illegible]	[illegible]	[illegible]	[illegible]	[illegible]	[illegible]	[illegible]	[illegible]	[illegible]
D [illegible]	[illegible]	[illegible]	[illegible]	[illegible]	[illegible]	[illegible]	[illegible]		
	[illegible]	[illegible]	[illegible]	[illegible]	[illegible]	[illegible]	[illegible]	[illegible]	[illegible]
	[illegible]	[illegible]	[illegible]	[illegible]	[illegible]	[illegible]	[illegible]	[illegible]	[illegible]
	[illegible]	[illegible]	[illegible]	[illegible]	[illegible]	[illegible]	[illegible]	[illegible]	[illegible]
	[illegible]	[illegible]	[illegible]	[illegible]	[illegible]	[illegible]	[illegible]	[illegible]	[illegible]
	[illegible]	[illegible]	[illegible]	[illegible]	[illegible]	[illegible]	[illegible]	[illegible]	[illegible]
	[illegible]	[illegible]	[illegible]	[illegible]	[illegible]	[illegible]	[illegible]	[illegible]	[illegible]
	[illegible]	[illegible]	[illegible]	[illegible]	[illegible]	[illegible]	[illegible]	[illegible]	[illegible]
	[illegible]	[illegible]	[illegible]	[illegible]	[illegible]	[illegible]	[illegible]	[illegible]	[illegible]
	[illegible]	[illegible]	[illegible]	[illegible]	[illegible]	[illegible]	[illegible]	[illegible]	[illegible]
	[illegible]	[illegible]	[illegible]	[illegible]	[illegible]	[illegible]	[illegible]	[illegible]	[illegible]
	[illegible]	[illegible]	[illegible]	[illegible]	[illegible]	[illegible]	[illegible]	[illegible]	[illegible]
	[illegible]	[illegible]	[illegible]	[illegible]	[illegible]	[illegible]	[illegible]	[illegible]	[illegible]
E [illegible]	[illegible]	[illegible]	[illegible]	[illegible]	[illegible]	[illegible]	[illegible]	[illegible]	[illegible]
	[illegible]	[illegible]	[illegible]	[illegible]	[illegible]	[illegible]	[illegible]	[illegible]	[illegible]
	[illegible]	[illegible]	[illegible]	[illegible]	[illegible]	[illegible]	[illegible]	[illegible]	[illegible]
	[illegible]	[illegible]	[illegible]	[illegible]	[illegible]	[illegible]	[illegible]	[illegible]	[illegible]
	[illegible]	[illegible]	[illegible]	[illegible]	[illegible]	[illegible]	[illegible]	[illegible]	[illegible]
	[illegible]	[illegible]	[illegible]	[illegible]	[illegible]	[illegible]	[illegible]	[illegible]	[illegible]
	[illegible]	[illegible]	[illegible]	[illegible]	[illegible]	[illegible]	[illegible]	[illegible]	[illegible]

Appendix III

Multichannel Analysis of Surface Waves (MASW) Studies

Equipment used

A 24-channel signal enhancement seismograph 'Geode' manufactured by M/S Geometrics Inc., USA was used in this study. It has a 24-bit A/D and 24-dB, single stage, instantaneous floating point (IFP) amplifier, followed by an A/D converter sampling at 31.25 microsecond intervals. The floating point number is fed to a 32-bit floating point digital signal processor (DSP) which performs multi-sample processing to increase the effective resolution and dynamic range. Maximum input signal is about 300mV p-p and input impedance is 20K ohms. It has in-built software for simple processing of both refraction and reflection data. Sample rate in the range of 31.25 to 2ms and selectable record length in the range of 200 ms to 32 seconds. The system can be triggered with a hammer switch, contact closure, contact open, external SEM amplifier, or positive or negative voltage. It includes digitally summing of repetitive shots into a 32-bit register, allowing thousands of stacks without clipping. Rolling is the added feature of this instrument.

Dispersion Curve and Inversion

Dispersion curves are displayed as phase velocity versus frequency and the relationship can be established by calculating the phase velocity from the linear slope of each component of the swept frequency record. The accuracy of a dispersion curve can be enhanced by the analysis and removal of noise on ground roll data. The accurate potential of each frequency component, a multichannel coherency measure (Yilmaz, 1987) can be applied to a ground roll seismogram. A frequency domain approach (Park, et al., 1998) for calculating the dispersion curve can also be used on impulsive data. The dispersion analysis is repeated till a good S/N ratio is achieved.

The V_s profiles are calculated using an iterative inversion process that requires the dispersion data and estimation of Poisson's ratio and density. A least-squares approach allows automation of the process (Xia, et al., 1999). After each iteration, only the shear wave velocity is updated with Poisson's ratio, density and model thickness remaining unchanged throughout the inversion. An initial model needs to be specified as a starting point for the iterative inversion process consists of velocity (P-wave and S-wave velocity), density, and thickness parameters (Venkateswarlu and [illegible], 2012). Each dispersion curve is individually inverted into depth velocity model. For inversion, four information parameters are required namely, density, V_p, V_s and thickness. The nearest possible values for density and V_s is estimated and included a-priori for a good inversion with an optimal number of iterations and error limits can also be defined (Sudarsanayana, 2007).

6. Computations Based on Shear Wave Velocity :-

The evaluation of dynamic properties of soil is significant in geotechnical earthquake engineering as they are highly nonlinear and can influence wave propagation. The parameters like V_s^{30}, stiffness, N values, predominant frequencies and corresponding amplifications, bedrock depth etc., are found to be of relevance. All these parameters can be determined based on shear wave velocity.

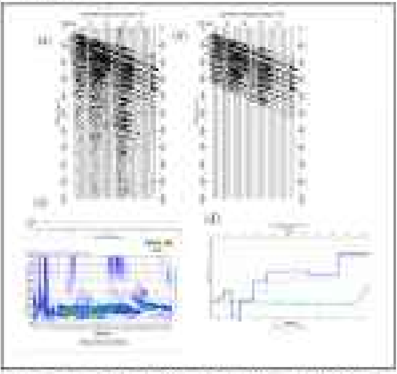

Figure 11: a) 24 channel raw field record, b) Pre-processed record after top and bottom mute, c) Dispersion curve after preprocessed record with extracted energy and d) Inversion of extracted dispersion

- Harmonic Mean Shear Wave Velocity

The classification of sites based on harmonic mean shear wave velocity is given by Federal Emergency Management Agency, (FEMA, 1997) and Uniform Building Code (UBC-ICBO 1997). V_s^{30} is accepted for site classification as per NEHRP classification and UBC classification (Dobry et al., 2000; Kanli et al., 2006). The harmonic mean shear wave velocity up to top 30m (V_s^{30}) is computed by using the equation (1).

$$V_s = \frac{\sum d_i}{\sum (d_i/v_i)} \quad --- (1)$$

Where $H = \sum d_i$ is cumulative depth in m, d_i and v_i denote the thickness (in meters) and shear wave velocity in m/s of the i^{th} formation or layer respectively, from a total of N layers, comprising the top 30m.

- Stiffness

The stiffness measured using field seismic method represents the maximum stiffness (G_{max}) (Matthews, et al., 1997). The maximum values of stiffness will therefore be measured using seismic methods by using the formula: $G = \rho V_s^2$ —— (2)

where ρ is the density of soil, V_s is the shear wave velocity measured using the MASW testing. For this reason the stiffness parameters measured in this manner are referred to as G_{max} and E_{max}. These parameters provide valuable benchmark against which other stiffness values measured in the laboratory or in situ can be compared.

- Liquefaction Potential

The liquefaction hazard is commonly associated with saturated sandy and silty soils having low plasticity and density. The controlling factors are soil type, density and water table. Liquefaction susceptibility is the capacity of soil to resist liquefaction and the presence of sandy layers at depths <10m and water table <10m. The liquefaction at depth decouple overlying soil layer from the underlying ground allowing its upper soil to oscillate back and forth and up and down in the form of ground waves. Centrifuge test suggests that for level ground, liquefaction cannot occur at a depth greater than 25–30m in a sandy soil deposit.

The safety factor from liquefaction is shown in Table below (Iwasaki, et al., 1982).

Liquefaction potential FS range

Factor of safety range	Description
<1	High
[illegible]	Moderate
[illegible]	Low
[illegible]	Nil
Non Liquefiable	Nil

Results from MASW studies

Profile DKM-1:

The S- wave velocity image with respect to depth pertaining to profile DKM-1 is presented in Fig. 2. This site is located near Jayanti Camp, Visakhapatnam, Marwadi Road. The profile is consisting of two layers sequentially from the surface. Shear wave velocities of the entire profile varies from 100 to 1200 m/s up to a depth of 30 m. Layer 1 up to a depth of 20 m from the surface with a velocity of 200 to 700 m/s might be pertains Dense Soil materials. A discrete low velocity formation (100 to 300 m/s) is identified as within the Dense Soil might be stiff soil with intrusion or filled sand and landslide debris material. This low- velocity formation is observed at shallow to deeper levels. The Consolidated Rock formation (layer 2) is noticed with a velocity of >700m/s below 20 m. depth. This formation not uniformly distributed throughout the profile. According to NEHRP code, observed layers (Fig. 2) are classified as Class C to B. The estimated V_{s30} is 470 m/s corresponds to Dense Soil formation classified as Class C (Table 3).

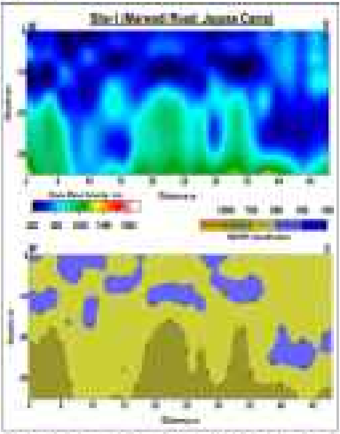

Figure 2. 2D Shear Wave Velocity Images of Profile DKM-1 (Top Panel) and corresponding Soil layers according NEHRP classification (Bottom Panel)

Profile 2MM-2

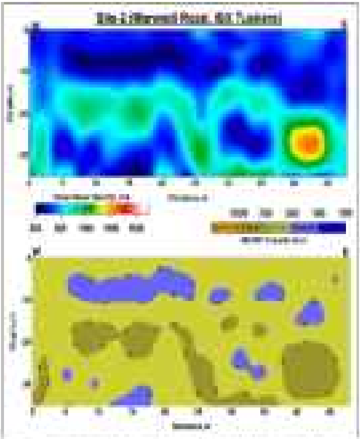

Profile JMM-1

The S-wave velocity image with respect to depth pertaining to profile JMM-1 is presented in Fig 4. This site is located at Marwadi Road. This profile is consisting of two layers sequentially from the surface. Shear wave velocities of the entire profile varies from 250 to 1140 m/s up to a depth of 40 m. Layer-1 is extending up to a depth to 40 m from the surface with a velocity of 360 to 760 m/s might be presence Dense Soil materials. A discrete low velocity formation (250 to 360 m/s) is identified within the Dense Soil might be cuff soil with saturation or filled sand and landslide debris material. In this section, the low velocity layer is spread at shallow levels (above 10m). The Consolidated Rock formation (layer-2) is noticed with a velocity of >760m/s below 20 m depth. This formation not uniformly distributed throughout the profile. According to NEHRP code, observed layers (Fig 4) are classified as Class D to B. The estimated V_s^{30} is 493 m/s corresponds to Dense Soil formation classified as Class-C (Table B1).

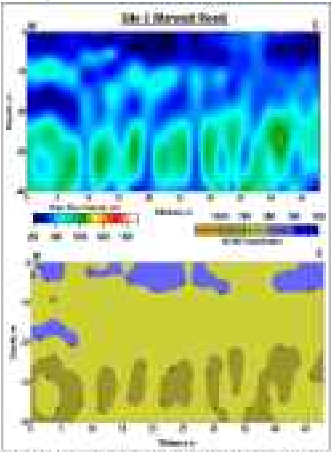

Figure 4: 2D Shear Wave Velocity Images of Profile JMM-1 (Top Panel) and corresponding Soil Property according NEHRP classification (Bottom Panel)

Profile 2MM-4

The 2-D shear wave velocity images with respect to depth pertaining to profile 2MM-4 is presented in Figure 5. This site is located at Shahbhari. This profile is consisting of two layers sequentially from the surface. Shear wave velocities of the entire profile varies from 250 to 2000 m/s up to a depth of 40 m. Layer-1 is extending up to a depth to 40 m from the surface with a velocity of 300 to 760 m/s might be presence Dense Soil materials. A discrete low velocity formation (250 to 300 m/s) is identified within the Dense Soil might be stiff soil with saturation or filled some sand/landslide debris material. In this section, the low velocity layer is spread at shallow locations (above 30m). The Consolidated Rock formation (layer-2) is noticed with a velocity of >760m/s at 35m depth. This formation are uniformly distributed throughout the profile. According to NEHRP code, observed layers (Figure 5) are classified as Class D to B. The estimated V_{s}^{30} is 497 m/s corresponds to Dense Soil formation classified as Class C (Table 8).

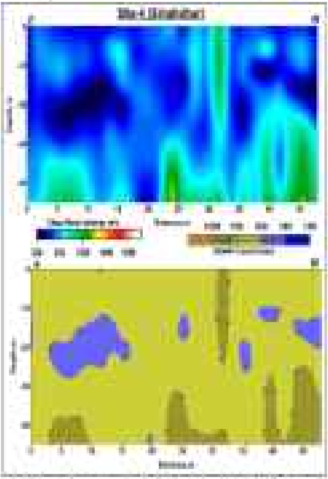

Figure 5: 2D Shear Wave Velocity Images of Profile 2MM-4 (Top Panel) and corresponding Soil Property according NEHRP classification (Bottom Panel)

Profile JMM-3

The S-wave velocity image with respect to depth pertaining to profile JMM-3 is presented in Figure 8. This site is located at Haringb Mandir Road, near PWD office. This profile is consisting of two layers sequentially from the surface. Shear wave velocities of the entire profile varies from 250 to 1000 m/s up to a depth of 40 m. Layer-1 is extending up to a depth of 40 m from the surface with a velocity of 300 to 780 m/s might be presents Dense Soil materials. A distinct low velocity formation (250 to 300 m/s) is identified within the Dense Soil might be stiff soil with saturation or filled sand and landslide debris material. In this section, this low velocity layer is spread at shallow to deeper levels. The Consolidated Rock formation (layer-2) is marked with a velocity of > 780m/s below 30 m depth. This formation not uniformly distributed throughout the profile. According to NEHRP code, observed layers (Figure 8) are classified as Class D to B. The measured V_{s30} is 450 m/s corresponding to Dense Soil formation classified as Class C (Table 8).

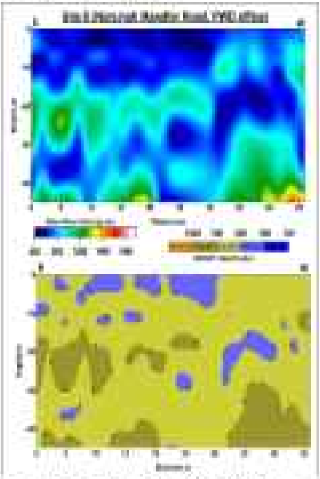

Figure 8: 2D Shear Wave Velocity Images of Profile JMM-3 (Top Panel) and corresponding Soil Regions according NEHRP classification (Bottom Panel).

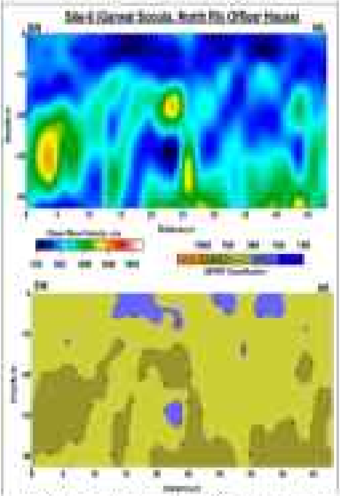

Profile JMM-8

The S- wave velocity image with respect to depth pertaining to profile JMM-8 is presented in Figure 8. This site is located at Adil Road near Basti Kadar [illegible] Stop. This profile is consisting of two layers sequentially from the surface. Shear wave velocities of the entire profile varies from 200 to 1400 m/s up to a depth of 30 m. Layer-1 is extending up to a depth to 20 m from the surface with a velocity of 500 to 760 m/s might be presence of dense soil materials. A continuous low velocity formation (200 to 500 m/s) is identified a within the Dense Soil might be stiff soil with intrusion of [illegible] and landslide debris material. In this section, this low velocity layer is spread from surface to a depth of 5m. The Consolidated Rock formation (layer 2) is noticed with a velocity of > 760m/s below 20 m depth. This formation not uniformly distributed throughout the profile. According to NEHRP code, observed layers (Figure 8) are classified in Class D to B. The estimated V_s^{30} is 482 m/s corresponds to Dense Soil formation classified in Class C (Table 8.2).

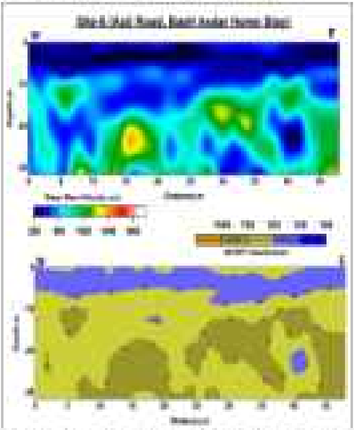

Figure 8.8 Shear Wave Velocity Images of Profile JMM-8 (Top Panel) and corresponding Soil Type(s) according NEHRP classification (Bottom Panel)

Profile [illegible]

The S-wave velocity image with respect to depth pertaining to profile [illegible] is presented in Figure 8. This site is located at [illegible] Bridge area near [illegible]. This profile is consisting of two layers sequentially from the surface. Shear wave velocities of the entire profile varies from 220 to 1100 m/s up to a depth of 40 m. Layer-1 is extending up to a depth of 40 m from the surface with a velocity of 250 to 700 m/s [illegible] material. No low velocity layer is observed with in the dense soil. The Consolidated Rock formation (layer-2) is noticed with a velocity of >700 m/s below 30 m depth. This formation are uniformly distributed throughout the profile. According to NEHRP code, observed layers (Figure 9) are classified as Class C to A. The estimated V_s^{30} is 400 m/s corresponds to Dense Soil formation classified as Class C (Table 8.1).

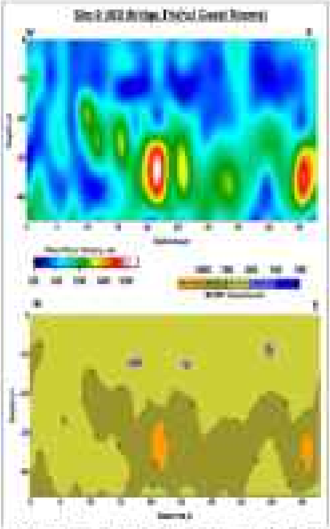

Figure 8. 2D Shear Wave Velocity Images of Profile [illegible] (Top Panel) and corresponding Soil Classes according NEHRP classification (Bottom Panel)

Profile ZkBM-10

The S-wave velocity image with respect to depth pertaining to profile ZkBM-10 is presented in Figure 28. This site is located in [illegible] from [illegible]. This profile is consisting of two layers sequentially from the surface. Shear wave velocities of the entire profile varies from 200 to 1700 m/s up to a depth of 30 m. Layer-1 is extending up to a depth of 20 m from the surface with a velocity of 300 to 760 m/s which may represent Dense Soil materials. A distinct low velocity formation (200 to 300 m/s) is identified within the Dense Soil might be stiff soil with saturation or filled sand and landslide debris material. In this section, this low velocity layer is [illegible] shallow to deeper levels. The Consolidated Rock formation (layer 2) is noticed with a velocity of >760 m/s at a depth of 20m and below the 20m depth. This formation are uniformly distributed throughout the profile. According to NEHRP code, observed layers (Figure 28) are classified as Class D to B. The estimated V_s^{30} is [illegible] m/s corresponds to Dense Soil formation classified as Class C (Table 5).

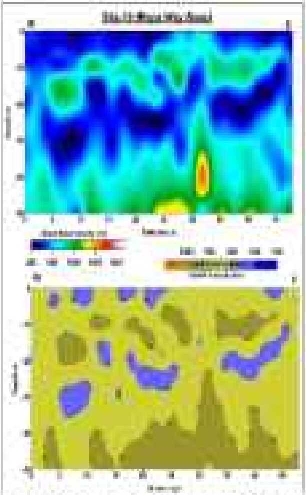

Figure 28: 2D Shear Wave Velocity Image of Profile ZkBM-10 (Top Panel) and corresponding 2D [illegible] NEHRP Classification (Bottom Panel)

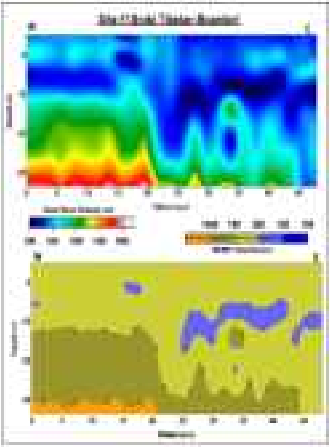

Profile JMM-13

The S-wave velocity image with respect to depth pertaining to profile JMM-13 is presented in Figure 22. This site is located at road at Bhaskar's Bhadi Palam. This profile is consisting of two layers sequentially from the surface. Shear wave velocities of the entire profile varies from 250 to 1000 m/s up to a depth of 30 m. Layer-1 is extending up to a depth of 20 m from the surface with a velocity of 300 to 700 m/s might be presents Dense Soil materials. A distinct low velocity formation (250 to 300 m/s) is identified within the Dense Soil might be stiff soil with saturation or filled sand and landslide debris material. In this section, the low velocity zone is spread in shallow levels (below 10 m). The Consolidated Rock formation (layer 2) is noticed with a velocity of >700 m/s at a depth of 20 m. This formation is not uniformly distributed throughout the profile. According to NEHRP code, observed layers (Figure 22) are classified as Class C to A. The estimated V_s^{30} is 461 m/s corresponds to Dense Soil formation classified as Class C (Table 3).

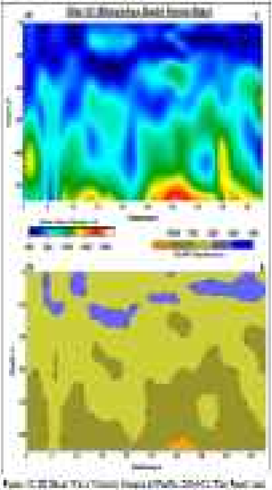

Figure 22: 2D Shear Wave Velocity Image of Profile JMM-13. The Bands and corresponding the Category according NEHRP classification (Table 3).

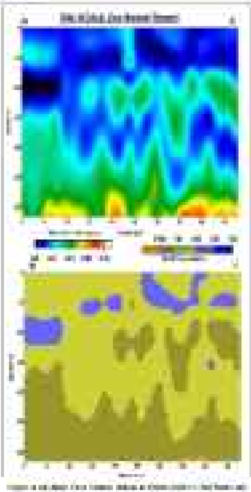

Appendix IV:

Ground Penetrating Radar (GPR) data profile:

Methodology

GPR survey is a portable non-destructive EM method that can produce high resolution subsurface images in near real time. GPR uses high frequency EM energy to transmit discrete pulses and receive the reflected signal (Reid, 2001). Similar to the reflection seismology, it makes use of the echo principle. A transmitter antenna on the ground surface sends a very short radar pulse, lasting only several nanoseconds. The path of the radar signal through the ground can be traced as a ray, which experiences refraction, reflection and diffraction at geological boundaries (usually the contacts of lithological formations and structural discontinuities) with notable dielectric contrast. The method is successfully in locating subsurface structural features such as caves, fractures, shear zones, ground water potential zones and [illegible] etc. (Overmeeren and Nicolo, [illegible]; Benson, 1995; Singh and Chouhan, 2000; Singh and Chouhan, 2002). It produces a cross-sectional image based on the propagation, reflection and scattering of EM waves across contrasting dielectric constant of the soil/rock, which depends on grain size, water content, porosity, etc.

The EM waves frequencies in GPR range from 10 MHz to 2.6 GHz and the smaller frequency offer greater penetration depth and vice versa (Reid, 2001; Mellett 1995; Singh and Chouhan, 2000, 2002). The penetration depth of the transmitted waves can be determined from the equation:

$$D = c t / \sqrt{E}$$

where D is the depth of penetration (m), c the velocity of light in free space, the t is a travel time (seconds), E is the dielectric constant.

In present study, SIR [illegible] GPR system with 100 MHz and 40 MHz central frequency antennas were used. Data was acquired in the continuous mode (distance mode). The data collection was done at [illegible] scans/sec and [illegible] scans/unit in horizontal scale and [illegible] samples/scan and [illegible] bits/sec in vertical scale. We used the conventional frequency setting for data acquisition, with high-pass equal to 1/6th the antenna frequency and low-pass higher than the antenna frequency. The dielectric value of the upper layer (relative permittivity of asphalt) was equal to 4-[illegible] was assigned with an estimated maximum depth of penetration to ~[illegible] m. The field data was processed using Radan 7 software with following steps: the time zero correction, background removal, finite impulse response (FIR), gain, stacking and signal filter. The time

... correction function was applied to the raw data to detect the ground wave peak position, followed by elimination of the portion prior to the time zero using time shift to bring initial data to exact ground surface. Background removal was applied to remove all the horizontal coherent noises using full pass background removal.

To increase the signal to noise ratio, low pass ([illegible] MHz) and high pass ([illegible] MHz) filters were applied. The values of filters were decided by the frequency spectrum of the neighbourhood region including spectrum peak. Exponential gain ([illegible]) with depth was applied to reduce the fluctuation of amplitude of traces, which reduces with depth. Horizontal stretching was applied to transfer the profile to its original scale. The processed data is reliable up to a certain depth, which is given by the signal floor. The fields data below the signal floor has been clipped from profiles displayed after final processing.

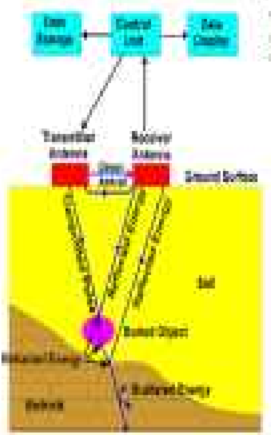

Fig. 2.1: Schematic diagram showing working principle of Ground Penetrating Radar (GPR).

GPR data along different profiles

Marvadi Region (JG1, JG-2 & JG-3)

Multiple ~300 m long profiles, namely JG1, JG2, and JG3, are obtained from the locations along the Marvadi Road (Figure 2c). The data is acquired using a 40 MHz frequency antenna with a depth of signal flow of ~40m (Figures 3a, 3b, and 3c). Topsoil (Layer-1) up to 4-5m depth is poorly saturated and does not cause signal attenuation. The second layer-2 up to 30 m depth is partially saturated debris with areas of dry colluvium largely correlated with the multiple vertical fractures which become wide at depth and extend up to ~40m from the surface. Many zones of inclined vertical surfaces with higher moisture also represent cracks and some progressively become horizontal mimicking Listric fault geometry. The third layer is largely [illegible] deformed. Apart from the natural structural features, cultural objects like underground pipes and nails are also delineated from the GPR sections. Vertical crack type signatures are identified at a distance of 2m, 25 m, and 50 m, apart from these minor cracks are also observed. A Prominent fractures are demarcated at deeper levels in JG-1 and JG-2 sections (Figure 3a and 3b). However, in section JG-3 (Figure 3c) a continuation of fractures is identified from the surface to the deeper level.

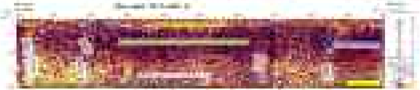

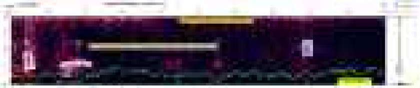

4.3. Singhdhar Region (30-4, 30-5, 30-6, 30-7a, and 7b)

Multiple ±100 m long profiles, namely 30-4 to 30-7, are obtained from the locations along the Singhdhar Road (Figure 31a to Figure 36). Topsoil (Layer-1) up to 4–5 m depth is poorly saturated and does not cause signal attenuation. The second layer (L2) up to ~15 m depth is partially saturated, laden with zones of dry columns largely correlated with the multiple vertical fissures which become wide at depth and extend up to ~6m from the surface. Many zones of discrete vertical surfaces with higher moisture also represent cracks and some progressively become horizontal mimicking Listric fault geometry. The third layer is largely saturation deficient.

A vertical crack-type signatures are identified at a distance of 5m, 8m, 38m, 50m, 73m, 95 m, 20 m, 88m, 74m and 95m (Figure 31 to 36). Apart from these a minor crack are also observed. In 30-4 (Figure 31) and a highly saturated zone at a distance of 15 to 25 m and 80 m to 100 m identified. These two saturated zones are divided with a partially saturated zone with cracks and fissures. In 30-5 (Figure 32), a horizontal saturated zone is observed from the surface to a depth of 12 m underlain by a saturation depletion dome. Here, fissures are observed below the 12 m depth. In 30-6 (Figure 33) section is similar to section 30-5. Figure 34 shows the GPR sections of 30-7a and 30-7b are forward and reverse direction. It is observed from the section a saturated soil is observed up to depth of 12m with fissures (at a distance of 5 m and 10 m). A saturation depletion dome are identified at depth of 12 m.

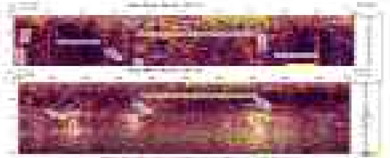

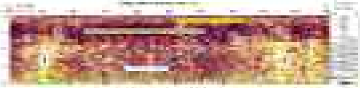

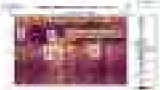

4.3 [illegible] (208 and 209)

Multiple ~100 m long profiles, namely 2D-1 to 2D-4, are obtained from the locations along the [illegible] Road (Figures 4a to 4d). Topsoil (Layer 1) up to ~1 m depth is poorly saturated and does not cause signal attenuation. The second layer (2 up to ~15 m depth) is partially saturated [illegible] with zones of dry columns largely coincident with the multiple vertical fissures which become wide at depth and extend up to ~4 m from the surface. Many zones of discrete vertical surfaces with higher [illegible] also represent cracks and some progressively become horizontal [illegible] geometry. The third layer is largely [illegible].

A vertical [illegible] type signature was identified at a distance of [illegible] and [illegible] (Figures 4c and 4d). Apart from these a minor crack are also observed. In 2D-2 (Figures 4b) a discrete saturated and unsaturated zones with mixtures of cracks and fissures are observed from surface to a depth of ~8 m. It is observed from the 2D-4 section (Figure 4d), most of the section occupied by a highly saturated zones with fissures and cracks.

4.4. Munshar Bagh Region (JS10, JS11, JS12, JS14, JS15, and JS16)

Multiple ~100 m long profiles, namely JS-11 to JS-16, are obtained from the locations along the Munshar Bagh (Figures 3a to 3f). Topsoil (Layer-1) up to ~4 m depth is poorly saturated and does not cause signal attenuation. The second layer-2 up to ~15 m depth is partially saturated debris with most of the stratum largely correlated with the multiple vertical fissures which become wide at depth and extend up to ~4 m from the surface. Many zones of discrete vertical surfaces with higher amplitude also represent cracks and some progressively become horizontal, maintaining Listric fault geometry. The basal layer is largely saturated deficient.

It is noted from the JS-11 (Figure 3a) a partially saturated zone is identified from the surface to a depth of 12 m underlain by a saturation depletion deficit. Very few cracks and fissures are observed in this section. In JS-12 section (Figure 3b) a sequential layering (poorly saturated, partially saturated debris, and saturated depletion deficit) are observed from the surface. A number of fissures and cracks are also observed in the partially saturated debris zone. Interestingly, it is observed in this section, a cuboid object as [illegible] pipes [illegible] the section at shallow to deep levels. The depth of these objects could not estimated from the GPR sections due to inference are also observed from the multiples which are like distance of the actual position of the object. In JS-13 section (Figure 3c), a vertical zone of fissure is observed at a distance of ~5 to 12 m from the surface to a depth of 12 m. This zone is juxtaposed in the all the observed sequential layers. Further a minor fissures and cracks are also observed at distance of 5 m, 22 m and 56 m. In JS-14 section (Figure 3d), minor fissures and cracks are also observed at distance of 5 m, 25 m, 35 m, 60, 70 m and 78 m. In JS-15 section (Figure 3e), a large vertical zone of fissure is observed at a distance of 35 to 45 m and 75 m to 80 m from the surface to a depth of 15 m. These zones are juxtaposed in the all the observed sequential layers. Further a minor fissures and cracks are also observed at distance of 2 m, and 15 m. JS-16 section (Figure 3f) occupied by a partially saturated zone up to a depth of 12 m with two fissure zones at a distance of 25 m and 60 m.

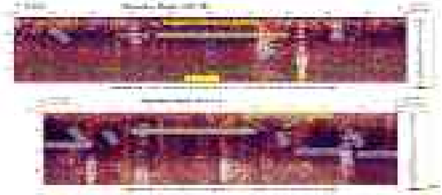

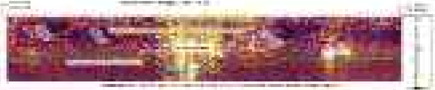

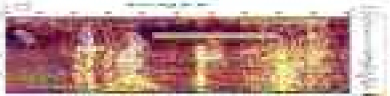

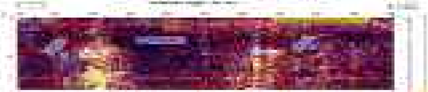

4.5. Sand Region (JS-18 to JS-24)

Multiple ~100 m long profiles, namely JS-18 to JS-24, are obtained from the locations along the [illegible] Bank (Figures 6a to 6f). Topsoil (Layer-1) up to ~7m depth is poorly saturated and does not cause signal attenuation. The second layer-2 up to ~20 m depth is partially saturated debris with zones of dry column largely correlated with the multiple vertical fissures which become wide at depth and extend up to ~10m from the surface. Many zones of discrete variable surfaces with higher resistivity also represent cracks and some progressively become horizontal mimicking listric fault geometry. The basal layer is largely saturated deltaic.

It is revealed from the JS-18 (Figure 6a), that fissures are observed at a distance of 3 m, 33, 45m, 53m, and 60m and minor fissures at a distance of 30m, 73m, and 77m. In the JS-19 section (Figure 6b), that fissures are observed at a distance of 15 m, 30, 38m, and 55m, and minor fractures at a distance of 65m, and 77. Further, a cultural object is observed at a distance of 73 m. This feature could be affected deep vertical pipes pathways for water. In the JS-20 section (Figure 6c), occupied by complete highly saturated zones are observed with a number of fissures and cracks. In the JS-21 section (Figure 6d), a continuous zone of the fissures is identified at a depth of 15m throughout the profile and it is extending up to a depth of 15 m. In the JS-22 section (Figure 6e), that fissures are observed at a distance of 20 m, 30, 38m, 53m, 73m, 83m, 95m, and some minor fractures. In the JS-23 section (Figure 6f), some fissures are identified throughout the profile. In the JS-23 section (Figure 6g), some fissures are identified throughout the profile. In the JS-24 section (Figure 6h), a wide fissure zone is identified in the western part of the profile up a distance of 30m. In this profile, the maximum zone is occupied by a highly saturated zone.

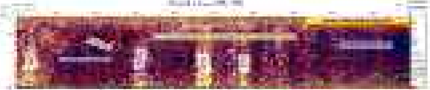

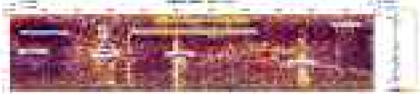

4.6.13 Road area

Two ~100 m long profiles, namely JO-27 and JO-28, are obtained from the locations along the Manchar Bagh (Figures 7a and 7b). Topsoil (Layer-1) up to ~4 [illegible] depth is poorly saturated and does not cause signal attenuation. The second layer (L2) up to ~20 m depth is partially saturated debris with zones of dry columns largely correlate with the multiple vertical fissures which become wide at depth and extend up to ~4 m from the surface. Many zones of discrete variable surfaces with higher continuity also represent cracks and zones progressively become horizontal mimicking Listric fault geometry. The basal layer is largely saturated deformed.

It is revealed from the JO-27 (Figure 7a), a narrow fissure zone is observed at a distance of 30 to 40 m. In JO-28 section (Figure 7b), a broad fissure zone is observed at a distance of 15 m. Further, a vertical object observed throughout the profile might be interference from underground power lines.

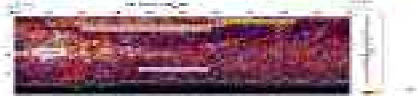

4.7. Repository area

40 to 60 m long profiles, namely [illegible] and [illegible], are obtained from the locations along the [illegible] Slope (Figures 8a and 8b). Topsoil (Layer-1) up to 4 [illegible] depth is poorly saturated and does not cause signal attenuation. The second layer-2 up to ~40 m depth is partially compacted debris with zones of dry columns largely coincident with the multiple vertical fissures which become wide at depth and extend up to ~4m from the surface. Many zones of discrete variable surfaces with higher resistivity also represent cracks and some progressively become horizontal mimicking Listric fault geometry. The basal layer is largely saturated [illegible] deformed.

To understand the cracks and fissures in this area GPR data was collected along the same profiles by using different antennas i.e. 40 MHz (Figure 8c) and 100 MHz (Figure 8d).

Several fissures within a short distance up to a depth of 30 m was observed in the repository area (Figure 8c). A highly saturated zone is observed at shallow levels up to a depth of 5m (Figure 8d).

References

Chianese, F.M. and Maio, E. 2012. Anthropogenic subsidence in the territory of the city of Naples (Southern Italy). Physics and Chemistry of the Earth, Parts A/B/C, 49, pp.95-102.

Benson, A.K., 1995. Applications of ground penetrating radar in assessing some geological hazards: examples of groundwater contamination, faults, cavities. Journal of applied Geophysics, 33(1-3), pp.177-193.

Singh, R. and Chandra, K., 2002. Exploration of subsurface mine conditions for a limestone mining area in India with ground penetrating radar. Environmental Geology, 41, pp.466-471.

Singh, R. and Chandra, K., 2002. Exploration of subsurface mine conditions for a limestone mining area in India with ground penetrating radar. Environmental Geology, 41, pp.466-471.

Neal, A., 2004. Ground-penetrating radar and its use in sedimentology: principles, problems and progress. Earth-science reviews, 66(3-4), pp.261-330.

Mellett, J.S., 1995. Ground penetrating radar applications in engineering, environmental management, and geology. Journal of Applied Geophysics, 33(1-3), pp.157-166.

Dobry, R., Borcherdt, R.D., Crouse, C.B., Idriss, I.M., Joyner, W.B., Martin, G.R., Power, M.S., Rinne and Seed, R.B. (2000). New site coefficients and site classification system used in recent building seismic code provisions, Earthquake Spectra, 16, No. 1, pp. 41-67, February.

Kanli, A.I., Tildy, P., Pronay, Z., Pinar and Hermann, L. (2006). VS30 mapping and soil classification for seismic site effect evaluation in Dinar region, SW Turkey, Geophysical J. Int., Vol. 165, pp.223-235.

Park, C.B., Xia, J., and Miller, R.D., (1998b). Ground roll as a tool to image near-surface anomaly: 68th Ann. Internat. Mtg., Soc. Expl. Geophys., Expanded Abstracts, p. 874-877.

Building Seismic Safety Council (BSSC), (2003). NEHRP Recommended Provisions for Seismic Regulations for New Buildings and Other Structures, Parts 1 and 2, FEMA-303, Federal Emergency Management Agency, Washington, D.C.

Federal Emergency Management Agency (FEMA), 1997. Multi Hazard Identification and Assessment. FEMA, Washington, D.C.

Seshunarayana, T., and Sundararajan, N., (2012). Determination of Shear Wave Velocity and Depth to Basement Using Multichannel Analysis of Surface Wave Technique. Journal of Geological Society of India. Vol. 80, pp. 488-494.

Seshunarayana, T., (2003). Seismic Survey for determination of Vp and Vs of shallow subsurface and bedrock depth in Jabalpur area, for use in microzonation studies. Tech Rep No. NGRI-2003-EXP-374, National Geophysical Research Institute, Hyderabad, India.

Xia, J., Miller, R.D., Park, C.B., (1999). Configuration of Near-Surface Shear-Wave Velocity by Inverting Surface Waves: Proceedings of the Symposium on the Application of Geophysics to Engineering and Environmental Problems, V. 99, pp. [illegible].

Yilmaz, O., (1987). Seismic data processing: Doherty, S. M., Ed.: Investigations in Geophysics, no. 2, Soc. of Expl. Geophys.